PERGAMON

International Journal of Solids and Structures 37 (2000) 2825–2857

INTERNATIONAL JOURNAL OF SOLIDS and STRUCTURES

www.elsevier.com/locate/ijsolstr

Canonical representations of complex vibratory subsystems: time domain Dirichlet to Neumann maps

Paul E. Barbone*, Aravind Cherukuri [1], Daniel Goldman [2]

Department of Aerospace and Mechanical Engineering, Boston University, Boston, MA 02215, USA

Received 9 June 1998; received in revised form 11 March 1999

Abstract

Large scale dynamic simulations can often be simplified by appropriately replacing large portions of the domain by a Dirichlet to Neumann, or DtN map (Givoli 1992. Numerical Methods for Problems on Infinite Domains, 1st ed. Elsevier, Amsterdam). Here we consider the problem of representing a linear dynamical subsystem by such a map. The exact DtN map is computed as a modal summation and its properties are studied. Bounds on the symbol of the DtN map in the Laplace domain are obtained. The exact map is then approximated, in particular in the high modal density regime. In the high modal density limit, we obtain the result that a subsystem can be accurately represented with just three parameters. Within such an approximation we obtain representations based on a maximum entropy representation, self-similar or fractal representation, and a rational function representation. The rational function representation leads to the interesting result that any complicated dynamical subsystem with a large number of degrees of freedom is asymptotically equivalent (in the limit of infinite modal density) to a single mass-dashpot-spring system. We end with numerical examples showing the efficiency of the rational function approximation.

Keywords: Fuzzy structure; Dynamics; Vibration; Substructure; Model reduction; Dynamic reduction; High modal density

1. Introduction

Substructuring and 'reduction' or 'condensation' procedures have been used to simplify large scale numerical calculations since the mid 1960s (Guyan, 1965; Hurty, 1965). In typical condensation procedures, one begins with a complete model of the so-called 'slave' subsystem, and projects the

* Corresponding author. Fax: +1-617-353-5866.
E-mail address: barbone@bu.edu (P.E. Barbone).
[1] Currently affiliated with Parametric Technologies Corporation, Waltham, MA.
[2] Currently affiliated with Biomedical Engineering Department, Johns Hopkins University.

0020-7683/00/$ - see front matter
PII: S0020-7683(99)00070-0

response of the slave subsystem onto a relatively small subspace. The subspace is typically developed from a combination of rigid body modes, dynamic modes, and constraint modes (Craig, 1995).

Such techniques are especially useful when the subsystem has relatively few eigenvalues in the frequency range of interest of a given simulation. Then the subsystem can be represented by relatively few component modes, and its response is relatively simple to simulate and to understand. We are mainly concerned here, however, with the opposite case: that is when within any frequency range of interest, a very large number of eigenvectors of the subsystem are necessary to accurately characterize its response. We consider such a subsystem to be *complicated*.[3] This limit has been examined in the context of a specific example by Weaver (1996, 1997) Strasberg and Feit (1996) Nagem et al. (1997) and in other special and more general cases by, Pierce et al. (1993), Pierce (1995a), Cherukuri and Barbone (1998), Goldman and Barbone (1996) and Barbone (1995, 1998).

Rather than the condensation approaches mentioned above, we choose to represent the substructure through its Dirichlet to Neumann, or DtN Map (Givoli, 1992). Givoli, Keller and coworkers have been very successful in using DtN maps to represent the 'difficult' parts of computational problems in many different settings, including: infinite domains (Keller and Givoli, 1989; Givoli and Keller, 1989, 1990), shell problems (Givoli, 1990), and cracks and corners (Givoli and Keller, 1992; Givoli and Rivkin, 1993).

In the context of dynamic substructure representation, the DtN map takes displacement histories on the boundary of the substructure into current forces/tractions applied at the same boundary. Accordingly, the forces are the Neumann data, and the displacements are the Dirichlet data. Given the exact DtN map representing a slave substructure, the presence of that substructure is exactly taken into account when computing the dynamics of the master structure.

Though exact DtN map representations of substructures may be available, approximate representations are often attractive. There are at least two reasons for this. First, the approximate representation may provide sufficient accuracy at greatly reduced computational cost. Second, and perhaps more importantly, an approximate representation may involve only a few gross parameters of the dynamical system, sometimes as few as three as we shall show. These parameters can be easily estimated, thus permitting simulations to be performed without detailed knowledge of the dynamic properties of the substructures. This is an especially important advantage when the substructure is very complicated.

In this paper, we consider the problem of constructing and approximating time-domain DtN map representations of very complicated substructures. We shall focus here on the special case of a substructure which is attached to the master through a single point. In Section 2 we formulate the problem to be solved in order to find the DtN map. We give the exact DtN map in Section 3, and discuss various of its properties in Section 4. These include bounds on the DtN map in the Laplace domain which are, we believe, presented for the first time here. We also derive various bounds on many of the gross dynamic properties of the subsystem in this section. We then move on to the special case of high modal density systems in Section 5. By expanding the DtN map asymptotically in powers of the modal spacing, we find that an approximate DtN map can be constructed that depends on as few as three parameters. We call these the 'effective dynamical parameters', and their identification represents one of the central contributions of this paper. On the basis of our high modal density theory, we consider three 'canonical representations' in Section 6. These are: the maximum entropy representation, the self-similar or fractal representation, and the rational function representation. The rational function representation leads to a startling equivalence: that undamped but sufficiently complicated substructures are asymptotically equivalent (in the limit or zero modal spacing) to a single spring-dashpot-mass

[3] Some authors refer to such subsystems as 'fuzzy substructures'.

system, up to simulation times proportional to the inverse of the modal spacing. Specific formulas for the coefficients of the reduced system are given. Finally, we give some examples applying our theory for complicated subsystems in Section 7.

2. Formulation

We consider a dynamical subsystem which has a quadratic potential energy function in the N degrees of freedom, x_n, $n = 1, \ldots, N$. We shall assume that the dynamical system is attached to the outside world at only one attachment point; see Fig. 1. The displacement of the attachment point from equilibrium is denoted by $x_0(t)$. We will denote by $f_0(t)$ the force that is applied to the attachment point. The 'DtN' condition that we will derive represents a map from $x_0(t)$ to $f_0(t)$. Thus, the effect of the dynamical subsystem can be included in a dynamical simulation by employing the following boundary condition at the attachment point

$$f_0(t) = \mathscr{M}[x_0(t)]. \tag{1}$$

Here, $\mathscr{M}$ denotes the DtN map.

In what follows, x_0 and x_n are purely unidirectional. The extension to many attachment points and three dimensional displacements follows in a future contribution.

In the case when $f_0 = 0$, we can write the potential energy function as

$$V(x_0, \mathbf{x}) = \frac{1}{2}[\mathbf{x} \cdot \mathbf{K}\mathbf{x} + 2x_0\boldsymbol{\kappa} \cdot \mathbf{x} + k_o x_0^2]. \tag{2}$$

Here, $\mathbf{x}$ is an N dimensional displacement vector, $\mathbf{K}$ is an $N \times N$ positive definite matrix, $\boldsymbol{\kappa}$ is an N dimensional vector of spring constants, and k_o is a coupling spring constant. The potential energy function must be invariant to rigid body translation (Pierce, 1995a). Therefore, for all α

$$V(x_0 + \alpha, \mathbf{x} + \alpha\boldsymbol{p}) = V(x_0, \mathbf{x}). \tag{3}$$

In Eq. (3), $\boldsymbol{p}$ is an N dimensional vector with each component equal to unity. Substituting Eq. (2) into

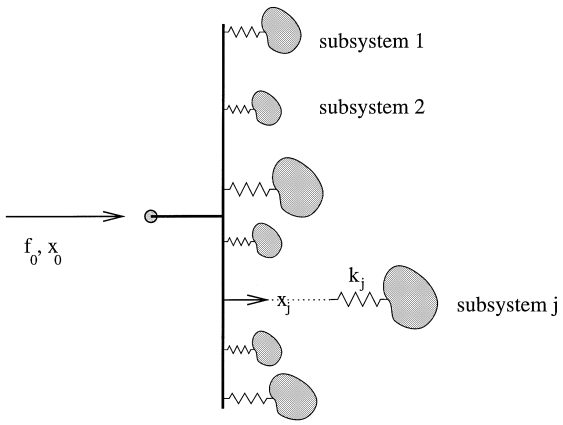

Fig. 1. A subsystem composed of many smaller subsystems. Each subsystem is connected at its attachment point to a light rigid rod. The rigid rod defines the attachment point of the new 'composite' subsystem. The attachment point displacement of the composite subsystem is $x_0(t)$, and the force required to specify that motion is $f_0(t)$.

Eq. (3) yields

$$\mathbf{Kp} = -\boldsymbol{\kappa} \tag{4}$$

$$k_o = -\boldsymbol{p} \cdot \boldsymbol{\kappa} = \mathbf{p} \cdot \mathbf{Kp}. \tag{5}$$

We introduce the positive definite mass matrix $\mathbf{M}$ which allows us to write the kinetic energy function as:

$$T(\dot{\mathbf{x}}) = \frac{1}{2}[m_o \dot{x}_0^2 + \dot{\mathbf{x}} \cdot \mathbf{M}\dot{\mathbf{x}}]. \tag{6}$$

Lagrange's dynamical equations of motion (Lanczos, 1986) given us the equations of motion for our system as:

$$\mathbf{M}\ddot{\mathbf{x}} + \mathbf{K}\mathbf{x}(t) = -\boldsymbol{\kappa} x_0(t) \tag{7}$$

$$m_o \ddot{x}_0 + \boldsymbol{\kappa} \cdot (\mathbf{x}(t) - \boldsymbol{p} x_0(t)) = f_0(t). \tag{8}$$

3. Exact DtN map

An exact DtN map can be constructed by solving Eq. (7) exactly and substituting the result into Eq. (8). An exact solution of Eq. (7) can be constructed in terms of a Green's function. The Green's function itself shall be found in terms of the modes of vibration of the dynamical subsystem.

3.1. The Green's function

The Green's function, $\boldsymbol{g}(t-\tau)$ satisfies

$$\mathbf{M}\ddot{\mathbf{g}}(t-\tau) + \mathbf{K}\mathbf{g}(t-\tau) = -\boldsymbol{\kappa}\delta(t-\tau), \tag{9}$$

$$\boldsymbol{g}(t-\tau) = \mathbf{0} \quad t < \tau. \tag{10}$$

Eq. (7), together with Eqs. (9) and (10) show that $\mathbf{x}(t)$ is given by

$$\mathbf{x}(t) = \int_{-\infty}^{t} \boldsymbol{g}(t-\tau) x_0(\tau)\, \mathrm{d}\tau. \tag{11}$$

We now solve Eq. (9) for $\boldsymbol{g}$ in terms of a normal mode expansion. We begin by introducing a change of dependent variables

$$\boldsymbol{g}(t) = \mathbf{M}^{-1/2}\mathbf{y}(t). \tag{12}$$

Here, $\mathbf{M}^{1/2}$ is the unique positive definite matrix which satisfies $\mathbf{M}^{1/2}\mathbf{M}^{1/2} = \mathbf{M}$. We shall not have the need to calculate $\mathbf{M}^{1/2}$ explicitly here. Substituting Eq. (12) into Eq. (9) and left multiplying both sides by $\mathbf{M}^{-1/2}$ yields

$$\ddot{\boldsymbol{y}}(t) + \mathbf{M}^{-1/2}\mathbf{K}\mathbf{M}^{-1/2}\mathbf{y}(t) = -\mathbf{M}^{-1/2}\boldsymbol{\kappa}\delta(t). \tag{13}$$

The matrix $\mathbf{M}^{-1/2}\mathbf{K}\mathbf{M}^{-1/2}$ is $N \times N$, symmetric and positive definite. It therefore possesses N distinct, orthonormal eigenvectors $\boldsymbol{\xi}^{(n)}$, $n = 1, \ldots, N$, and N (not necessarily distinct) positive eigenvalues ω_n^2:

$$\mathbf{M}^{-1/2}\mathbf{K}\mathbf{M}^{-1/2}\boldsymbol{\xi}^{(n)} = \omega_n^2\boldsymbol{\xi}^{(n)} \tag{14}$$

Since $\boldsymbol{\xi}^{(n)}$ span R^N, we can write

$$y(t) = \sum_{n=1}^{N}\boldsymbol{\xi}^{(n)}z_n(t). \tag{15}$$

We now substitute Eq. (15) into Eq. (13) and make use of the orthonormality of $\boldsymbol{\xi}^{(n)}$ to obtain

$$\ddot{z}_n(t) + \omega_n^2 z_n(t) = -\boldsymbol{\xi}^{(n)} \cdot \mathbf{M}^{-1/2}\boldsymbol{\kappa}(t). \tag{16}$$

Further, causality requires

$$z_n(t) = 0 \quad t < 0. \tag{17}$$

Solving Eq. (16) subject to the condition (17) yields

$$z_n(t) = -\frac{1}{\omega_n}\boldsymbol{\xi}^{(n)} \cdot \mathbf{M}^{-1/2}\boldsymbol{\kappa}\ \sin(\omega_n t) \quad t \geq 0. \tag{18}$$

We obtain $\boldsymbol{g}(t)$ by using Eq. (18) in Eqs. (15) and (12) to find, for $t > 0$

$$\boldsymbol{g}(t) = -\mathbf{M}^{-1/2}\sum_{n=1}^{N}\frac{1}{\omega_n}\boldsymbol{\xi}^{(n)}[\boldsymbol{\xi}^{(n)} \cdot \mathbf{M}^{-1/2}\boldsymbol{\kappa}]\ \sin(\omega_n t). \tag{19}$$

With $\boldsymbol{g}(t)$ determined, the exact DtN map follows directly using Eqs. (11) and (8):

$$f_0(t) = m_o\ddot{x}_0(t) - \boldsymbol{\kappa} \cdot \boldsymbol{p}x_0(t) - \int_{-\infty}^{t}\boldsymbol{\kappa} \cdot \mathbf{M}^{-1/2}\sum_{n=1}^{N}\frac{1}{\omega_n}\boldsymbol{\xi}^{(n)}[\boldsymbol{\xi}^{(n)} \cdot \mathbf{M}^{-1/2}\boldsymbol{\kappa}]\ \sin\omega_n(t-\tau)\, x_0(\tau)\, \mathrm{d}\tau \tag{20}$$

Eq. (20) can be simplified by utilizing the concept of modal mass. O'Hara and Cunniff (1963) define the modal mass as (see also generalization in Pierce (1995a) and Cherukuri and Barbone (1998))

$$m_n = (\boldsymbol{p} \cdot \mathbf{M}^{-1/2}\boldsymbol{\xi}^{(n)})^2. \tag{21}$$

From the definition of $\boldsymbol{\xi}^{(n)}$, we note that

$$\mathbf{M}^{-1/2}\mathbf{K}\mathbf{M}^{-1/2}\boldsymbol{\xi}^{(n)} = \omega_n^2\boldsymbol{\xi}^{(n)}. \tag{22}$$

We left multiply Eq. (22) by $\boldsymbol{\kappa} \cdot \mathbf{K}^{-1}\mathbf{M}^{1/2}$, and use Eq. (4) to find

$$\boldsymbol{\kappa} \cdot \mathbf{M}^{-1/2}\boldsymbol{\xi}^{(n)} = -\omega_n^2\boldsymbol{p} \cdot \mathbf{M}^{1/2}\boldsymbol{\xi}^{(n)}. \tag{23}$$

We now use Eqs. (23) and (21) to simplify Eq. (20) and obtain

$$f_0(t) = m_o\ddot{x}_0(t) + k_o x_0(t) - \int_{-\infty}^{t}\sum_{n=1}^{N}m_n\omega_n^3\ \sin\omega_n(t-\tau)\, x_0(\tau)\, \mathrm{d}\tau. \tag{24}$$

4. Properties of DtN map

The exact DtN map, Eq. (24), has many interesting properties which we now describe. These include relations among the various coefficients appearing in Eq. (24), as well as the behavior of the Laplace transform of the DtN map in the complex plane.

4.1. The properties of the modal masses

O'Hara and Cunniff (1963) show that the sum of the modal masses defined as in Eq. (21) is equal to the total mass of the substructure, i.e.

$$\sum_{n=1}^{N} m_n = M_T \tag{25}$$

For completeness of our presentation, we show a similar proof here. From Eq. (21) and the orthonormality of $\boldsymbol{\xi}^{(n)}$, we have:

$$\sum_{n=1}^{N} m_n = \sum_{n=1}^{N} (\boldsymbol{p}\cdot\mathbf{M}^{1/2}\boldsymbol{\xi}^{(n)})^2 = \sum_{n=1}^{N} (\boldsymbol{p}\cdot\mathbf{M}^{1/2}\boldsymbol{\xi}^{(n)})(\boldsymbol{p}\cdot\mathbf{M}^{1/2}\boldsymbol{\xi}^{(n)}) = \boldsymbol{p}\cdot\mathbf{M}^{1/2}\mathbf{M}^{1/2}\boldsymbol{p} = \boldsymbol{p}\cdot\mathbf{M}\mathbf{p} = M_T. \tag{26}$$

A relation that is stated by neither O'Hara and Cunniff (1963) nor Pierce (1995a) is that between the attachment stiffness k_o and the modal masses. To show this, we consider the sum:

$$\begin{aligned}
\sum_{n=1}^{N} \omega_n^2 m_n &= \sum_{n=1}^{N} \omega_n^2 (\boldsymbol{p}\cdot\mathbf{M}^{1/2}\boldsymbol{\xi}^{(n)})^2 = \sum_{n=1}^{N} \omega_n^2 (\boldsymbol{p}\cdot\mathbf{M}^{1/2}\boldsymbol{\xi}^{(n)})(\boldsymbol{p}\cdot\mathbf{M}^{1/2}\boldsymbol{\xi}^{(n)}) \\
&= \sum_{n=1}^{N} \omega_n^2 \left(\boldsymbol{p}\cdot\left(\frac{1}{\omega_n^2}\mathbf{K}\mathbf{M}^{-1/2}\boldsymbol{\xi}^{(n)}\right)\right)(\boldsymbol{p}\cdot\mathbf{M}^{1/2}\boldsymbol{\xi}^{(n)}) \\
&\text{(by Eq. (22))} = \boldsymbol{p}\cdot\mathbf{K}\mathbf{M}^{-1/2}\mathbf{M}^{1/2}\boldsymbol{p} = k_o \quad \text{(by Eqs. (4) and (5))}.
\end{aligned} \tag{27}$$

Here, we again used the orthonormality of the $\boldsymbol{\xi}^{(n)}$.

The two parameters M_T and k_o can be used to define a 'bulk' frequency scale for the subsystem. Thus we define Ω, the effective or bulk or gross frequency parameter of the subsystem as:

$$\Omega^2 = k_o/M_T. \tag{28}$$

4.2. The DtN map in the Laplace domain

We now consider the Laplace transform of Eq. (24) and the resulting DtN map in the transform domain. To that end, we first introduce the following definitions:

$$F_0(s) = \int_0^\infty f_0(t)\, \mathrm{e}^{-st}\, \mathrm{d}t \tag{29}$$

$$X_0(s) = \int_0^\infty x_0(t)\, \mathrm{e}^{-st}\, \mathrm{d}t \tag{30}$$

Multiplying Eq. (24) by e^{-st} and integrating with respect to t then yields:

$$F_0(s) = s^2 m_o X_0(s) + K(s) X_0(s) \tag{31}$$

Here we have introduced $K(s)$, the symbol of the DtN operator under Laplace transformation. It is given by the function:

$$K(s) = k_o - \int_0^\infty \sum_{n=1}^{N} m_n \omega_n^3 \sin(\omega_n t)\, e^{-st}\, dt. \tag{32}$$

In obtaining Eq. (31), we assumed that both $x_0(t) = 0$ and $f_0(t) = 0$ for all $t < 0$. Further, we assumed that

$$x_0(0) = 0; \quad x_0'(0) = 0. \tag{33}$$

The transform of the DtN operator, $K(s)$ can be easily computed. Evaluating the integral indicated in Eq. (32) for $\mathscr{R}(s) > 0$ yields

$$K(s) = k_o - \sum_{n=1}^{N} m_n \frac{\omega_n^4}{s^2 + \omega_n^2}. \tag{34}$$

We use Eq. (34) to continue the definition of $K(s)$ over the entire s-plane. We note by inspection that $K(s)$ has no singularities in the complex s plane except those at the points $s_n = \pm i\omega_n$.

4.2.1. Bounds on K(s)

Here we find it convenient to consider $K(s)$ as a function of s^2. That is, we consider the function:

$$K_2(s^2) \equiv K(s) = k_o - \sum_{n=1}^{N} m_n \frac{\omega_n^4}{s^2 + \omega_n^2} \tag{35}$$

We observe from Eq. (35) that $K_2(z)$ $(z = s^2)$ is a rational function of z with singularities only at the points $z_n = -\omega_n^2 < 0$; i.e. only on the negative real axis.

Further, we note that the analytic continuation of $K_2(z)$ into the whole of the z-plane is *Herglotz* (Bender and Orszag, 1978; p. 358); i.e. $\mathscr{I}(K_2(z)) < 0 \Leftrightarrow \mathscr{I}(z) < 0$, $\mathscr{I}(K_2(z)) > 0 \Leftrightarrow \mathscr{I}(z) > 0$ and $\mathscr{I}(K_2(z)) = 0 \Leftrightarrow \mathscr{I}(z) = 0$. To show this, we let $z = x + iy$ (x and y are real), and obtain from Eq. (35)

$$K_2(z) = k_o - \sum_{n=1}^{N} m_n \frac{\omega_n^4}{(x + \omega_n^2)^2 + y^2}[(x + \omega_n^2) - iy]. \tag{36}$$

The fact that $K_2(z)$ is Herglotz thus follows by inspection, noting that $m_n > 0$ and ω_n is real. Finally, we note that $K_2(z) \to k_o$ as $z \to \infty$ for any arg z. These properties together are sufficient to guarantee that $K_2(z)$ is bounded by its Padé approximants (Bender and Orszag, 1978, p. 406).

Following the notation of Bender and Orszag (1978), and N–M Padé approximation shall be denoted by $P_M^N(z)$. That is

$$K_2(z) \approx P_M^N(z) \equiv \frac{\sum_{n=0}^{N} a_n z^n}{\sum_{m=0}^{M} b_m z^m}. \tag{37}$$

Without loss of generality, b_0 is chosen to be 1. Clearly, the fact that $K_2(z)$ is rational implies that the Padé sequence will converge to $K_2(z)$ for N and M sufficiently large. Smaller values of N and M, however, provide upper and lower bounds on $K_2(z)$:

$$P_N^{N-1}(z) \le P_{N+1}^N(z) \le K_2(z) \le P_{N+1}^{N+1}(z) \le P_N^N(z) \quad \forall N,\ z > 0 \tag{38}$$

Thus, each diagonal or nearly diagonal Padé approximant provides a bound on $K_2(z)$: the higher order the approximant, the sharper the bound.

Padé sequences can be developed from the Taylor expansion of $K_2(z)$ about any point. In particular, the values of $z = 0$ or $z = \infty$ correspond to the physical limits of low and high frequency response, respectively. Thus, if the low or high frequency limiting behavior of the system is known or can be accurately estimated, then a Padé approximation can be formed there. Such estimates can be used to provide bounds on equipment models that will be presented later.

4.3. Low and high frequency approximate DtN maps

Eq. (24) represents the exact DtN map for the dynamical subsystem under consideration. In general, $2N$ parameters are required to characterize the subsystem. When N is small, Eq. (24) can be conveniently used directly. In practice, however, N can be arbitrarily large. In such situations, it is often beneficial to consider approximations to Eq. (24) in which the DtN map can be accurately represented by relatively few effective parameters. In this section, we discuss two limiting cases in which this is possible. These are the special cases when the excitation is either of very low frequency or very high frequency. These provide approximations valid not only at small and large s^2, but by the results of Section 4.2, also bounds on the behavior of $K(s)$ along the entire real s-line. The bounds thus found can be used to find bounds and interrelations between the bulk or effective subsystem parameters, as we show below.

4.3.1. Low frequency limit

When the frequency of the excitation is much lower than the natural frequencies of the subsystem, then the inertia of the subsystem is negligible to a first approximation. To obtain an approximate DtN map in this case, we rewrite Eq. (7) as

$$\mathbf{K}\mathbf{x}(t) = -\boldsymbol{\kappa} x_0(t) - \mathbf{M}\ddot{\mathbf{x}}. \tag{39}$$

Solving Eq. (39) by iteration yields

$$\mathbf{x}(t) = -\mathbf{K}^{-1}\boldsymbol{\kappa} x_0(t) + \mathbf{K}^{-1}\mathbf{M}\mathbf{K}^{-1}\boldsymbol{\kappa}\ddot{x}_0(t) - \mathbf{K}^{-1}\mathbf{M}\mathbf{K}^{-1}\mathbf{M}\mathbf{K}^{-1}\boldsymbol{\kappa}\frac{\mathrm{d}^4 x_0(t)}{\mathrm{d}t^4} + \cdots \tag{40}$$

We now substitute Eq. (40) into Eq. (8) and simplify using Eq. (5) to obtain

$$f_0(t) = m_o\ddot{x}_0(t) + M_T\ddot{x}_0(t) - \boldsymbol{p}\cdot\mathbf{M}\mathbf{K}^{-1}\mathbf{M}\mathbf{p}\frac{\mathrm{d}^4 x_0(t)}{\mathrm{d}t^4} + \cdots \tag{41}$$

Here, we have used the relation $M_T = \boldsymbol{p}\cdot\mathbf{M}\mathbf{p}$, which represents the total mass in the subsystem. We note that to leading order, the force is merely accelerating the subsystem as a rigid body.

Alternatively, we can derive a relation equivalent to Eq. (41) in the Laplace domain. Expanding Eq. (31) in a Taylor series about $s = 0$ yields

$$F_0(s) = \left[s^2 m_o + K(0) + sK'(0) + \frac{1}{2}s^2K''(0) + \frac{1}{6}s^3K'''(0) + \frac{1}{24}s^4K^{(iv)}(0) + \cdots\right]X_0(s). \tag{42}$$

The individual coefficients in the series can be evaluated from Eqs. (34) and (27). Then Eq. (42) simplifies to:

$$F_0(s) = \left[s^2(m_o + M_T) - s^4 \sum_{n=1}^{N} \frac{m_n}{\omega_n^2} + s^6 \sum_{n=1}^{N} \frac{m_n}{\omega_n^4} - \cdots \right] X_0(s) \tag{43}$$

Inverse transforming Eq. (43), and using Eq. (21) yields Eq. (41).

It is interesting to consider a Padé approximation of $K(s)$ obtained from this expansion. We can construct the P_1^1 and P_2^1 Padé approximants (about $z = 0$) of $K_2(z) = K(s)$ by matching their asymptotic expansions about $z = 0$ to the coefficients in Eq. (43). This yields

$$P_2^1(s^2) \leq K(s) \leq P_1^1(s^2) \tag{44}$$

$$P_2^1(s^2) = \frac{s^2 M_T^2}{M_T + s^2 \sum_{n=1}^{N} (m_n/\omega_n^2) + s^4 \left[\left(\sum_{n=1}^{N} (m_n/\omega_n^2) \right)^2 - M_T \sum_{n=1}^{N} (m_n/\omega_n^4) \right] / M_T} \tag{45}$$

$$P_1^1(s^2) = \frac{s^2 M_T^2}{M_T + s^2 \sum_{n=1}^{N} (m_n/\omega_n^2)}. \tag{46}$$

Eq. (44) provides not only approximations of $K(s)$, but also upper and lower bounds for all $s^2 > 0$.

Eq. (44) can also be used to find relations between the different coefficients that appear in those equations. For example, evaluating Eq. (44) at $s = \infty$, and using Eqs. (28) and (55) yields:

$$\Omega^2 \sum_{n=1}^{N} (m_n/\omega_n^2) \leq M_T. \tag{47}$$

Further, recognizing that $P_1^1 \geq P_2^1 \ \forall s^2$ gives us:

$$\left(\sum_{n=1}^{N} (m_n/\omega_n^2) \right)^2 \geq M_T \sum_{n=1}^{N} (m_n/\omega_n^4). \tag{48}$$

These results shall be used later.

4.3.2. High frequency limit

Alternatively, the time scale of the excitation may be much higher than any of the natural frequencies of the dynamical subsystem. In this case, the inertia term in Eq. (7) dominates. We rewrite Eq. (7), therefore, as

$$\mathbf{M}\ddot{\mathbf{x}}(t) = -\boldsymbol{\kappa} x_0(t) - \mathbf{K}\mathbf{x} \tag{49}$$

$$\mathbf{M}\ddot{\mathbf{x}}(t) \approx -\boldsymbol{\kappa} x_0(t) \tag{50}$$

Taking two time derivatives of Eq. (8) and simplifying using Eq. (50) yields

$$\ddot{f}_0(t) = m_o x_0^{(iv)}(t) + k_o \ddot{x}_0(t) - \boldsymbol{\kappa} \cdot \mathbf{M}^{-1} \boldsymbol{\kappa} x_0(t). \tag{51}$$

Carrying the process still further yields:

$$f_0^{(iv)}(t) = m_o x_0^{(vi)}(t) + k_o x_0^{(iv)}(t) - \boldsymbol{\kappa} \cdot \mathbf{M}^{-1} \boldsymbol{\kappa} \ddot{x}_0(t) + \boldsymbol{\kappa} \cdot \mathbf{M}^{-1} \mathbf{K} \mathbf{M}^{-1} \boldsymbol{\kappa} x_0(t). \tag{52}$$

At very high frequencies, the last term in Eq. (51) can be neglected yielding

$$\ddot{f}_0(t) = m_o x_0^{(iv)}(t) + k_o \ddot{x}_0(t). \tag{53}$$

From Eq. (53), we see that in this regime the force is resisted primarily by the mass at the attachment point and the elasticity in the equipment mount. Based on the interpretation of Eq. (53), we refer to the quantity k_o as the 'high-frequency stiffness'.

It is again interesting to consider the identical approximation in the Laplace domain. By doing so, we shall obtain further bounds on $K(s)$. Taking the Laplace transform of Eq. (52) and noting Eq. (31) yields

$$F_0(s) = s^2 m_o X_0(s) + K(s) X_0(s) \tag{54}$$

$$K(s) \sim k_o - \boldsymbol{\kappa} \cdot \mathbf{M}^{-1} \boldsymbol{\kappa} s^{-2} + \boldsymbol{\kappa} \cdot \mathbf{M}^{-1} \mathbf{K} \mathbf{M}^{-1} \boldsymbol{\kappa} s^{-4} + o(s^{-6}) \quad s \to \infty \tag{55}$$

From the expansion (55), we can form the P_1^1 and P_1^0 Padé approximants, this time about the point $s = \infty$. Thus we obtain:

$$P_1^0(s^2) \le K(s) \le P_1^1(s^2) \tag{56}$$

$$P_1^0(s^2) = \frac{k_o^2}{k_o + \boldsymbol{\kappa} \cdot \mathbf{M}^{-1} \boldsymbol{\kappa} s^{-2}} \tag{57}$$

$$P_1^1(s^2) = \frac{k_o \boldsymbol{\kappa} \cdot \mathbf{M}^{-1} \boldsymbol{\kappa} + [(\boldsymbol{\kappa} \cdot \mathbf{M}^{-1} \boldsymbol{\kappa})^2 - k_o \boldsymbol{\kappa} \cdot \mathbf{M}^{-1} \mathbf{K} \mathbf{M}^{-1} \boldsymbol{\kappa}] s^{-2}}{\boldsymbol{\kappa} \cdot \mathbf{M}^{-1} \boldsymbol{\kappa} + \boldsymbol{\kappa} \cdot \mathbf{M}^{-1} \mathbf{K} \mathbf{M}^{-1} \boldsymbol{\kappa} s^{-2}} \tag{58}$$

Again, we have not only approximations of $K(s)$, but also bounds for all $s^2 \ge 0$. Eq. (56) implies that Eq. (58) must be non-negative at $s = 0$. This gives us:

$$(\boldsymbol{\kappa} \cdot \mathbf{M}^{-1} \boldsymbol{\kappa})^2 \ge k_o \boldsymbol{\kappa} \cdot \mathbf{M}^{-1} \mathbf{K} \mathbf{M}^{-1} \boldsymbol{\kappa}. \tag{59}$$

Expanding Eq. (57) in the neighborhood of $s = 0$, and using Eqs. (43) and (56) yields

$$k_o^2 s^2 \le M_T \boldsymbol{\kappa} \cdot \mathbf{M}^{-1} \boldsymbol{\kappa} s^2. \tag{60}$$

Eqs. (59) and (60) can be rewritten in terms of the modal masses and natural frequencies. To do so, we use Eqs. (4), (21) and (22) to find:

$$\boldsymbol{\kappa} \cdot \mathbf{M}^{-1} \boldsymbol{\kappa} = \sum_{n=1}^{N} m_n \omega_n^4 \tag{61}$$

$$\boldsymbol{\kappa}\cdot\mathbf{M}^{-1}\mathbf{K}\mathbf{M}^{-1}\boldsymbol{\kappa}=\sum_{n=1}^{N}m_n\omega_n^6. \tag{62}$$

Combining Eqs. (59)–(62) (and using Eq. (28) as necessary) yields bounds on the modal sums:

$$M_T\Omega^4\le\sum_{n=1}^{N}m_n\omega_n^4 \tag{63}$$

$$\left[\sum_{n=1}^{N}m_n\omega_n^4\right]^2\ge k_o\sum_{n=1}^{N}m_n\omega_n^6 \tag{64}$$

Eq. (64) shows that the behavior of the higher order moment ($\Sigma m_n\omega_n^6$) is determined by the behavior of lower order moments. Eq. (63) shall be used in a later section.

5. High modal density

In the last section, we simplified the form of the exact DtN map, Eq. (24), by making assumptions regarding the form of the excitation (i.e. high or low frequency). In this section, we instead make an assumption regarding the complexity of the dynamical subsystem and thereby simplify the DtN map.

As noted earlier, the form of the DtN map in Eq. (24) is appropriate when the subsystem has few modes. In that case, the subsystem can be reasonably categorized as simple. On the other hand, when the subsystem has many modes in the frequency band of interest, i.e. is complicated, we seek an alternate representation that is more efficiently developed and evaluated.

Below, we change the sum in Eq. (24) to an integral over frequency. We then approximate the kernel of the frequency integral and bound the resulting error. Making the error bound as small as possible identifies a sequence of parameters that govern the dynamics of the subsystem. Our analysis indicates that these parameters are fundamental in describing the dynamics of the subsystem. The identification of these parameters is one of the main contributions contained in this paper.

5.1. Replacing sum by integral

When the modes of the subsystem are closely spaced in frequency, the sum over modes in Eq. (24) can be accurately approximated by an integral. Such a substitution is the basis of the fuzzy structure representations of Pierce et al. (1993). We shall also make use of the Pierce et al. (1993) notion of mass as a function of natural frequency.

Unlike Pierce et al., we *exactly* replace the sum over modes with an integral over a frequency parameter. To effect this replacement, we first introduce the generalized function, $m(\omega)$, defined by

$$\frac{\mathrm{d}m}{\mathrm{d}\omega}(\omega)=\sum_{n=1}^{N}m_n\delta(\omega-\omega_n) \tag{65}$$

$$m(0)=0 \tag{66}$$

Using Eq. (65) in the exact DtN map Eq. (24), allows us to rewrite that exact relation as

$$f_0(t)=m_o\ddot{x}_0(t)+k_ox_0(t)-\int_{-\infty}^{t}\int_0^{\infty}\frac{\mathrm{d}m(\omega)}{\mathrm{d}\omega}\omega^3\ \sin(t-\tau)x_0(\tau)\,\mathrm{d}\omega\,\mathrm{d}\tau. \tag{67}$$

5.1.1. Properties of $m(\boldsymbol{\omega})$

The function $m(\omega)$ inherits its properties from the modal masses in terms of which it is defined. Using Eq. (65) in Eqs. (26) and (27) yields directly

$$\int_0^\infty \frac{\mathrm{d}m}{\mathrm{d}\omega}(\omega)\,\mathrm{d}\omega = M_T \tag{68}$$

$$\int_0^\infty \omega^2 \frac{\mathrm{d}m}{\mathrm{d}\omega}(\omega)\,\mathrm{d}\omega = k_o. \tag{69}$$

In addition, those inequalities derived in Section 4.3 have counterparts in terms of $m(\omega)$.

5.2. High modal density approximation

When the modes of the subsystem are closely spaced in frequency, the kernel in the integral operator in Eq. (67) is rapidly varying. Under those conditions, the action of the operator can be simulated in terms of another integral operator with a smooth kernel. With this motivation in mind, we therefore consider splitting $m(\omega)$ into a 'smooth' part and a rapidly varying part as follows:

$$m(\omega) = \bar{m}(\omega) + m_e\left(\frac{\omega}{\epsilon}\right). \tag{70}$$

Here, we have introduced the parameter ϵ defined by

$$\epsilon = \Delta\omega/\Omega_{99} \ll 1. \tag{71}$$

$\Delta\omega$ is taken to be a measure of the modal spacing, for example

$$\Delta\omega = \max_n(\omega_n - \omega_{n-1})$$

or the average over all n of $(\omega_n - \omega_{n-1})$. Thus ϵ is a non-dimensional measure of the modal spacing. Ω_{99} is defined as the lowest frequency for which $m(\Omega_{99}) \geqslant .99M_T$. An approximate DtN map (or *fuzzy structure* approximation) is obtained by neglecting the $m_e(\omega)$ term in Eq. (70) and replacing $m(\omega)$ by $\bar{m}(\omega)$ in Eq. (67). The key to obtaining an *accurate* approximate DtN map lies in choosing $\bar{m}(\omega)$ appropriately.

We note that Eq. (70) leaves $\bar{m}(\omega)$ unspecified in its relation to $m(\omega)$. Thus we are considering the action of any continuous $\bar{m}(\omega)$ as an approximation for the action of $m(\omega)$. This notion is in contrast to the presentation of Cherukuri and Barbone (1998), who require $\bar{m}(\omega)$ to be the limit of $m(\omega)$ as $\epsilon \to 0$. Obviously, some choices of $\bar{m}(\omega)$ will lead to better approximations of the DtN map than others. In order to yield an accurate DtN map, some properties of the exact $m(\omega)$ must be duplicated in $\bar{m}(\omega)$. Precisely what aspects of $m(\omega)$ must be duplicated in $\bar{m}(\omega)$ in order to accurately represent the dynamics of the subsystem is determined below, in an error analysis.

5.3. Error bounds

5.3.1. Error analysis

To obtain an approximate DtN map, we substitute Eq. (70) into Eq. (67) to write:

$$f_0(t) = m_o\ddot{x}_0(t) + k_o x_0(t) - \int_0^t \int_0^\infty \frac{\mathrm{d}\bar{m}}{\mathrm{d}\omega}(\omega)\omega^3 \;\sin\omega(t-\tau)\, x_0(\tau)\,\mathrm{d}\omega\,\mathrm{d}\tau + \mathrm{error}(t) \tag{72}$$

$$\text{error}(t) = -\int_0^t \int_0^\infty \frac{\mathrm{d}}{\mathrm{d}\omega}\left[m_e\left(\frac{\omega}{\epsilon}\right)\right]\omega^3 \ \sin\omega(t-\tau)\, x_0(\tau)\, \mathrm{d}\omega\, \mathrm{d}\tau. \tag{73}$$

Here we have made the assumption that

$$x_0(t) \equiv 0 \quad \forall t < 0 \tag{74}$$

We shall now analyze the error in the force, error(t). In what follows, we shall assume that all functions are regular enough to carry out our calculations, and that all integrals and limits are defined. Integrating Eq. (73) by parts three times with respect to t and using Eq. (74) yields:

$$\text{error}(t) = -\int_0^\infty \frac{\mathrm{d}}{\mathrm{d}\omega}\left[m_e\left(\frac{\omega}{\epsilon}\right)\right]\left\{\omega^2 x_0(t) - x_0''(t) + \int_0^t \cos\omega(t-\tau)\, x_0'''(\tau)\, \mathrm{d}\tau\right\} \mathrm{d}\omega. \tag{75}$$

In terms of a new integration variable $v = \omega/\epsilon$, Eq. (75) can be rewritten as

$$\begin{aligned}\text{error}(t) = &\int_0^\infty \frac{\mathrm{d}m_e}{\mathrm{d}v}(v)\, \mathrm{d}v\, x_0''(t) - \epsilon^2 \int_0^\infty v^2 \frac{\mathrm{d}m_e}{\mathrm{d}v}(v)\, \mathrm{d}v\, x_0(t) \\ &- \int_0^t \left\{\int_0^\infty \frac{\mathrm{d}m_e}{\mathrm{d}v}(v)\ \cos\ \epsilon v(t-\tau)\, \mathrm{d}v\right\} x_0'''(\tau)\, \mathrm{d}\tau.\end{aligned} \tag{76}$$

We now introduce the following integrals of $m_e(\omega)$:

$$m_1(v) = \int_0^v m_e(v')\, \mathrm{d}v' \tag{77}$$

$$m_n(v) = \int_0^v m_{n-1}(v')\, \mathrm{d}v' \tag{78}$$

Integration by parts with respect to v allows us to write:

$$\begin{aligned}&\int_0^\infty \frac{\mathrm{d}m_e}{\mathrm{d}v}(v) \cos\epsilon v t\, \mathrm{d}v = m_e(v) \cos\epsilon v t\, |_{v=\infty} + \epsilon t m_1(v) \sin\epsilon v t\, |_{v=\infty} + \\ &\quad \cdots + (-1)^n \epsilon^{2n} t^{2n} m_{2n}(v) \cos\epsilon v t\, |_{v=\infty} + (-1)^n \epsilon^{2n+1} t^{2n+1} \int_0^\infty m_{2n+1}(v) \sin\epsilon v t\, \mathrm{d}v\end{aligned} \tag{79}$$

Here we have integrated by parts an odd number of times. One can, of course, integrate by parts an even number of times to obtain a similar result. The expansion indicated in Eq. (79) can be continued indefinitely, provided that the integrals at each stage converge. This convergence can be guaranteed for any $m(\omega)$ by an appropriate choice of $\bar{m}(\omega)$. In order for the limits (at $v = \infty$) indicated in Eq. (79) to exist, we require:

$$\lim_{v\to\infty} m_e(v) = 0 \tag{80}$$

$$\lim_{v\to\infty} m_j(v) = 0 \quad j = 1, \ \ldots, \ 2n \tag{81}$$

Substituting Eqs. (79)–(81) (with $n \geq 2$) into Eq. (76) now allows us to write error(t) as

$$\text{error}(t) = (-1)^{n+1}\epsilon^{2n+1}\int_0^t\int_0^\infty m_{2n+1}(v)\ \sin\ \epsilon v(t-\tau)\ \mathrm{d}v(t-\tau)^{2n+1}x_0'''(\tau)\ \mathrm{d}\tau. \tag{82}$$

5.3.2. Error bound

We now seek to bound error(t). To that end, we note

$$\begin{aligned}
\text{error}(t) &\le \left|(-1)^{n+1}\epsilon^{2n+1}\int_0^t\int_0^\infty m_{2n+1}(v)\sin\epsilon v(t-\tau)\ \mathrm{d}v(t-\tau)^{2n+1}x_0'''(\tau)\ \mathrm{d}\tau\right| \\
&\le \epsilon^{2n+1}t^{2n+1}\left|\int_0^\infty m_{2n+1}(v)\int_0^t \sin\epsilon v(t-\tau)x_0'''(\tau)\ \mathrm{d}\tau\ \mathrm{d}v\right| \\
&\le \epsilon^{2n+2}t^{2n+1}\left|\int_0^\infty vm_{2n+1}(v)\int_0^t \cos\epsilon v(t-\tau)x_0''(\tau)\ \mathrm{d}\tau\ \mathrm{d}v\right| \\
&\le \epsilon^{2n+2}t^{2n+1}\int_0^\infty\ |\ vm_{2n+1}(v)\ |\ \int_0^t\ |\ \cos\epsilon v(t-\tau)x_0''(\tau)\ |\ \mathrm{d}\tau\ \mathrm{d}v \\
&\le \epsilon^{2n+2}t^{2n+1}\int_0^\infty\ |\ vm_{2n+1}(v)\ |\ \mathrm{d}v\int_0^t\ |\ x_0''(\tau)\ |\ \mathrm{d}\tau \\
&\le \epsilon^{2n+2}t^{2n+1}\int_0^\infty\ |\ vm_{2n+1}(v)\ |\ \mathrm{d}v\int_0^t \mathrm{d}\tau\ |\ x_0''(\max)\ | = \epsilon^{2n+2}(t)^{2n+2}C_{2n+1}\ |\ x_0''(\max)\ |
\end{aligned} \tag{83}$$

Here, we have introduced the constant C_{2n+1} which is defined as

$$C_{2n+1} = \int_0^\infty\ |\ vm_{2n+1}(v)\ |\ \mathrm{d}v. \tag{84}$$

We note that for any $m(\omega)$, $\bar{m}(\omega)$ can always be chosen in such a way that C_{2n+1} exists. Further, the error grows with time as t^{2n+2}. Thus, no matter how small ϵ may be, the error becomes significant at a time $t = O(\epsilon^{-1})$. We note, however, that up to this point in the derivation we have neglected all forms of dissipation. If the subsystem under consideration has a small amount of dissipation (as shown by Cherukuri and Barbone, 1998) then the error will remain bounded for all time. In essence, this requires that all transient motion of $x_0(t)$ has stopped before the error has had a chance to accumulate.

5.3.2.1. The source of the error. The accumulation of error in this approximation is due to approximations of the phase of the individual modes. Replacing the exact DtN map, Eq. (24), by the approximation (72) can be thought of as replacing the individual term in Eq. (24) by the following integral:

$$m_n\omega_n^3\ \sin\ \omega_n(t-\tau) \approx \frac{1}{\omega_n\epsilon}\int_{\omega_n(1-\epsilon)/2}^{\omega_n(1+\epsilon)/2}\bar{m}(\omega)\omega^3\ \sin\ \omega(t-\tau)\ \mathrm{d}\omega \tag{85}$$

This approximation is valid only as long as the sine terms in the integral remain in phase with each other. To show this, we approximate the integral on the right of Eq. (85) in the following manner:

$$\frac{1}{\omega_n\epsilon}\int_{\omega_n(1-\epsilon)/2}^{\omega_n(1+\epsilon)/2}\bar{m}(\omega)\omega^3\ \sin\ \omega(t-\tau)\ \mathrm{d}\omega \approx \bar{m}(\omega_n)\omega_n^3\frac{1}{\omega_n\epsilon}\int_{\omega_n(1-\epsilon)/2}^{\omega_n(1+\epsilon)/2}\ \sin\ \omega(t-\tau)\ \mathrm{d}\omega \tag{86}$$

$$\approx \frac{-\bar{m}(\omega_n)\omega_n^{n3}}{\omega_n\epsilon(t-\tau)} \cos\ \omega(t-\tau)\ |_{\omega_n(1-\epsilon)/2}^{\omega_n(1+\epsilon)/2} \tag{87}$$

$$\approx \frac{\bar{m}(\omega_n)\omega_n^3}{\omega_n\epsilon(t-\tau)} 2\ \sin\ \omega_n(t-\tau)\ \sin(\omega_n\epsilon(t-\tau)/2) \tag{88}$$

$$\approx \frac{\bar{m}(\omega_n)\omega_n^3}{\omega_n\epsilon(t-\tau)} (\omega_n\epsilon(t-\tau)/2 - \omega_n^3\epsilon^3(t-\tau)^3/12) 2\ \sin\ \omega_n(t-\tau) \tag{89}$$

$$\approx \bar{m}(\omega_n)\omega_n^3\ \sin\ \omega_n(t-\tau)(1-\omega_n^2\epsilon^2(t-\tau)^2/6) \tag{90}$$

Therefore, we see that the error is due to accumulation of frequency approximations in the substitution of the sum for the integral. Thus, there is no need to appeal to any argument based on limiting dissipation (Weaver, 1997).

5.4. Effective dynamical parameters

Eqs. (80) and (81) state the conditions under which the error in the DtN map is bounded (see Eq. (83)). Through Eq. (70) these conditions specify certain restrictions on $\bar{m}(\omega)$ in its relation to $m(\omega)$. In satisfying these conditions, we shall identify several effective dynamical parameters which characterize a given dynamical subsystem.

To do so, we first consider the nth moment of the mass-frequency distribution $\mathrm{d}m_e/\mathrm{d}v\ (v)$

$$I_n = \int_0^\infty v^n \frac{\mathrm{d}m_e}{\mathrm{d}v}(v)\ \mathrm{d}v. \tag{91}$$

We now integrate Eq. (91) by parts to obtain

$$I_n = \sum_{j=0}^{n} (-1)^j v^{n-j} m_j(v). \tag{92}$$

Thus we conclude that conditions (80) and (81) are equivalent to

$$\int_0^\infty v^j \frac{\mathrm{d}m_e}{\mathrm{d}v}(v)\ \mathrm{d}v = 0, \quad j = 0,\ \ldots,\ 2n. \tag{93}$$

From the definition of $m_e(\omega/\epsilon)$ in Eq. (70), we obtain

$$\int_0^\infty v^j \frac{\mathrm{d}m_e}{\mathrm{d}v}(v)\ \mathrm{d}v = 0 \Leftrightarrow \int_0^\infty \omega^j \left(\frac{\mathrm{d}m}{\mathrm{d}\omega}(\omega) - \frac{\mathrm{d}\bar{m}}{\mathrm{d}\omega}(\omega) \right) \mathrm{d}\omega = 0. \tag{94}$$

Using the definition of $m(\omega)$, Eq. (65), in Eq. (94) yields

$$\int_0^\infty \omega^j \frac{\mathrm{d}\bar{m}}{\mathrm{d}\omega}(\omega)\ \mathrm{d}\omega = \sum_{n=1}^{N} \omega_n^j m_n. \tag{95}$$

Eq. (95) shows that in order to accurately represent a dynamical subsystem in a simulation, one must

choose the moments of $\bar{m}(\omega)$ to agree with those of the subsystem itself. These parameters, the frequency moments of the modal masses, are in this way fundamental in describing a system's dynamical response. We call them the 'effective dynamical parameters'.

5.4.1. Physical interpretation of effective parameters

For this section, and through the rest of this paper, we shall consider the special case of $n = 1$ (cf Eq. (81)). That is, we shall require that

$$\int_0^\infty \frac{\mathrm{d}\bar{m}}{\mathrm{d}\omega}(\omega)\,\mathrm{d}\omega = \sum_{n=1}^{N} m_n = M_T \tag{96}$$

$$\int_0^\infty \omega\frac{\mathrm{d}\bar{m}}{\mathrm{d}\omega}(\omega)\,\mathrm{d}\omega = \sum_{n=1}^{N} \omega_n m_n = \eta_o \tag{97}$$

$$\int_0^\infty \omega^2\frac{\mathrm{d}\bar{m}}{\mathrm{d}\omega}(\omega)\,\mathrm{d}\omega = \sum_{n=1}^{N} \omega_n^2 m_n = k_o. \tag{98}$$

Here we have used the results of Eqs. (25) and (27). We recall that M_T is the total mass of the subsystem, while k_o is the 'high frequency stiffness'. In Eq. (97) we have introduced the quantity η_o, which we shall call the 'effective dissipation' of the subsystem.

Eq. (83) with $n = 1$ shows that if one chooses $\bar{m}(\omega)$ to correctly represent the total mass M_T, high frequency stiffness k_o, and the effective dissipation η_o of a subsystem, then the error incurred in a dynamical simulation will be bounded by

$$\mathrm{error}(t) \le (\epsilon t)^4 C_5 \mid x_0''(\max) \mid . \tag{99}$$

From Eqs. (96)–(98) we can see that with each dynamical subsystem, we can associate a total mass and two frequencies. In what follows, we shall find it convenient to represent a subsystem in terms of its 'frequency' parameter Ω, (cf Eq. (28)) and 'damping' parameter α_0, which is defined by

$$\alpha_0 = \eta_o / M_T \Omega. \tag{100}$$

In Appendix A, we show that $\alpha_0 \le 1$ for all discrete dynamical systems.

6. Modeling dynamical subsystems: canonical representations

6.1. Canonical representations

In the last section, we determined those parameters of a dynamical subsystem that are important to describe the dynamics of that subsystem. That is, we determined which features of $m(\omega)$ must be duplicated in $\bar{m}(\omega)$ in order to accurately reproduce the force at the attachment point. Beyond the specification of the effective parameters just described, however, $\bar{m}(\omega)$ remains unspecified up to now.

In this section, we consider several canonical representations of dynamical subsystems that are based on different modeling perspectives. By 'representation', we mean a function $\bar{m}(\omega)$ which is used in the approximate DtN map, Eq. (72). In the rest of this section we consider different choices for $\bar{m}(\omega)$ which have prescribed values of M_T, η_o, and k_o. Each choice differs in its functional dependence on ω, but

nevertheless satisfies conditions (96)–(98). Therefore, each choice will yield accurate results in a dynamical simulation as specified in Eq. (99). Thus the specific choice of $\bar{m}(\omega)$ as described here is more a matter of taste or ease of application than of accuracy.

The three canonical functions we shall describe are derived from different perspectives. In the first, we shall derive an optimal representation based on information theory. The calculation presented below is motivated by and is similar in both spirit and detail to that presented by Pierce (1995b). We include it as one perspective to obtain a canonical $\bar{m}(\omega)$. In the second approach, we consider the form of $\bar{m}(\omega)$ to be a self-similar function of frequency. This leads to a non-linear functional equation which we solve for the function $\bar{m}(\omega)$. The third approach, the rational function representation, is motivated by the resulting simplicity of the approximate DtN map. It leads to a very satisfying physical analogy, which is presented in Section 6.4.3.

In what follows, we shall find it convenient to work in terms of a non-dimensional mass distribution function. Thus we introduce the non-dimensional frequency v and non-dimensional mass distribution $\mu(v)$ as follows:

$$v = \omega/\Omega \tag{101}$$

$$\mu(v) = \frac{\Omega}{M_T}\frac{\mathrm{d}\bar{m}}{\mathrm{d}\omega}(\omega). \tag{102}$$

In terms of Eqs. (101) and (102), the three conditions (96)–(98) take the form:

$$\int_0^\infty \mu(v)\,\mathrm{d}v = 1 \tag{103}$$

$$\int_0^\infty v\mu(v)\,\mathrm{d}v = \alpha_0 \tag{104}$$

$$\int_0^\infty v^2\mu(v)\,\mathrm{d}v = 1. \tag{105}$$

6.2. Maximum entropy formulation

6.2.1. Derivation of $\boldsymbol{\mu}(v)$

Because of the normalization property (103) of $\mu(v)$, we may think of this function in the abstract sense as a probability distribution. Following up on this line of thinking, we may also consider the conditions (104) and (105) as constraints on $\mu(v)$. Thus we seek to find a $\mu(v)$ that maximizes the 'entropy' or 'uncertainty' subject to the constraints that Eqs. (104) and (105) are satisfied. The uncertainty or entropy function for $\mu(v)$ can be written as (Pierce, 1995b):

$$H[\mu] = -\int_0^\infty \mu(v)\ \log(\mu(v))\,\mathrm{d}v. \tag{106}$$

We wish to find $\mu(v)$ such that H is stationary subject to the conditions (103)–(105). Therefore, we introduce the functional $\Pi[\mu]$ defined by

$$\Pi[\mu] = H[\mu] - \lambda_0\left(\int_0^\infty \mu \, \mathrm{d}v - 1\right) - \lambda_1\left(\int_0^\infty v\frac{\mathrm{d}\bar{m}}{\mathrm{d}\omega}(\omega)\, \mathrm{d}v - \alpha_0\right) - \lambda_2\left(\int_0^\infty v^2\frac{\mathrm{d}\bar{m}}{\mathrm{d}\omega}(\omega)\, \mathrm{d}v - 1\right). \tag{107}$$

Here, λ_0–λ_2 are Lagrange multipliers enforcing the constraints.

Making Π stationary with respect to μ, λ_0, λ_1, and λ_2 leads to Eqs. (103)–(105) and:

$$\int_0^\infty \delta\mu[\log\ \mu - 1 + \lambda_0 + \lambda_1 v + \lambda_2 v^2]\, \mathrm{d}v = 0 \tag{108}$$

Eq. (108) leads directly to the result

$$\mu(v) = \ \exp(1 - \lambda_0 - \lambda_1 v - \lambda_2 v^2). \tag{109}$$

6.2.2. Evaluating the coefficients, $\boldsymbol{\lambda}_0$, $\boldsymbol{\lambda}_1$, $\boldsymbol{\lambda}_2$

Substituting Eq. (109) into Eqs. (103)–(105) and rearranging yields the following equations for λ_0, λ_1 and λ_2:

$$1 = A\ \mathrm{e}^{\lambda_1^2/4\lambda_2}\frac{1}{2}\sqrt{\frac{\pi}{\lambda_2}}\ \mathrm{erfc}\left(\frac{\lambda_1}{2\sqrt{\lambda_2}}\right) \tag{110}$$

$$\alpha_0 = \frac{A - \lambda_1}{2\sqrt{\lambda_2}} \tag{111}$$

$$1 = \sqrt{\frac{1}{\lambda_2}}\left[\frac{1}{2} + \frac{\lambda_1^2}{4\lambda_2} - \frac{A\lambda_1}{2\lambda_2}\right] \tag{112}$$

$$A = \ \mathrm{e}^{1-\lambda_0} \tag{113}$$

Given α_0, Eqs. (110)–(112) are to be solved for λ_0–λ_2. These values are then to be substituted into Eq. (109) to obtain $\mu(v)$. In order to solve Eqs. (110)–(112), we combine them to write a single equation for the variable $c = \lambda_1/2\sqrt{\lambda_2}$:

$$(\alpha_0 + c)\sqrt{\pi}\ \exp(c^2)\ \mathrm{erfc}(c) = 1. \tag{114}$$

Once c is determined from Eq. (114), $A/\sqrt{\lambda_2}$ can be found from Eq. (111). Finally, λ_2 is obtained from Eq. (112). We note that it is easy to verify that for any values of $0 < \alpha_0 \leq 1$, Eq. (114) has a solution.

6.2.3. Implementation of maximum entropy representation

In order to get the DtN map associated with the Maximum Entropy Representation of $\mathrm{d}\bar{m}/\mathrm{d}\omega(\omega)$, we substitute Eq. (109) (in dimensional form) into Eq. (72) to write

$$f_0(t) = k_o x_0(t) - \int_0^t \boldsymbol{\kappa}(t-\tau)x_0(\tau)\, \mathrm{d}\tau, \tag{115}$$

$$\boldsymbol{\kappa}(t) = M_T A\int_0^\infty \omega^3\ \exp(-\lambda_1\omega/\Omega - \lambda_2\omega^2/\Omega^2)\ \sin\ \omega(t)\, \mathrm{d}\omega. \tag{116}$$

We note that λ_1 may be positive or negative, but λ_2 is strictly positive. We now evaluate the integral in Eq. (116) by writing $\sin(\omega t)$ as $\mathscr{I}\{e^{i\omega t}\}$ and integrating three times by parts to obtain

$$\boldsymbol{\kappa}(t) = -\frac{\Omega^4\lambda_1}{4\lambda_2^3}\Omega t + \frac{\Omega^4}{8\lambda_2}\sqrt{\frac{\pi}{\lambda_2}}\, e^{(\lambda_1^2-\Omega^2t^2)/4\lambda_2} \times \mathscr{I}\left\{(i\Omega t-\lambda_1)\left[3+\frac{1}{2\lambda_2}(i\Omega t-\lambda_1)^2\right][\right.$$
$$\left.\operatorname{erfc}((i\Omega t-\lambda_1)/2\sqrt{\lambda_2})]\, e^{-2i\lambda_2\Omega t}\right\} \tag{117}$$

The error function is defined by $\operatorname{erfc}(z) = (2/\sqrt{\pi})\int_z^\infty e^{-t^2}\, dt$ (Abramowitz and Stegun, 1972).

In the form of Eq. (117), $\boldsymbol{\kappa}(t)$ is difficult to use since the error function must be evaluated for complex argument. Of course, given the values of λ_1 and λ_2, this calculation could be done as a preprocess and the result tabulated. For more complicated functions of $\boldsymbol{\kappa}(t)$, this would be recommended. For the special case of $\lambda_1 = 0$, the error function drops out of the formulation.

6.3. Self-similar formulation

Here we formulate and solve the problem of determining the 'limiting' $\bar{m}'(\omega)$ in a complicated subsystem. The subsystem is imagined to be made up of a collection of smaller 'minor' subsystems, each of which, in turn, is made up of a collection of still smaller minor subsystems, and so on. As the subsystems become more and more complicated, we hope to find a limiting form of the $dm/d\omega(\omega)$ function.

To each minor subsystem, we shall prescribe three parameters: M_j, η_j, and k_j. Further, we define a 'frequency' and 'damping factor' for each minor subsystem defined as $\Omega_j = \sqrt{k_j/M_j}$, and $\alpha_{0j} = \eta_j/M_j\Omega_j$, respectively. In the Laplace domain, the DtN map for each subsystem can be written as:

$$F_j(s) = M_j\Omega_j^2 K(s/\Omega_j, \alpha_{0j})X(s). \tag{118}$$

If the minor subsystems are sufficiently complicated that their representation has reached its limiting form, then the function K will be *the same function for all the subsystems comprising the whole*. This is the essential assumption on which the following is based.

We now consider a subsystem comprised of many smaller subsystems as depicted in Fig. 1. The sum of the forces in springs j must balance the force f_0, thus

$$f_0 = \sum_{j=1} f_j. \tag{119}$$

Also, the displacements of each of the subsystems are identical

$$x_0 = x_j \quad j = 1, 2, \ldots \tag{120}$$

Combining Eqs. (118)–(120) allows us to write

$$M_0\Omega_0^2 K(s/\Omega_0, \alpha_0)X_0(s) = \sum_{j=1} M_j\Omega_j^2 K(s/\Omega_j, \alpha_0)X_0(s) \tag{121}$$

We require Eq. (121) to hold for arbitrary $X_0(s)$, which we can therefore cancel from both sides.

We now pass to the limit in which the number of subsystems becomes infinite. For convenience, we non-dimensionalize all frequencies with respect to Ω_0, and all masses with respect to M_0. Therefore we make the following replacements in Eq. (121):

$$\sigma = s/\Omega_0 \tag{122}$$

$$\Omega_j = \omega_j \Omega_0 \tag{123}$$

$$M_j = M_0 \frac{\mathrm{d}\bar{m}}{\mathrm{d}\omega}(\omega)\bigg|_{\omega=\omega_j} \mathrm{d}\omega \tag{124}$$

$$\sum_{j=1} = \int_0^\infty \tag{125}$$

Thus we obtain an integral equation for $\mathrm{d}\bar{m}/\mathrm{d}\omega(\omega)$:

$$K(\sigma, \alpha_0) = \int_0^\infty \frac{\mathrm{d}\bar{m}}{\mathrm{d}\omega}(\omega) K(\sigma/\omega, \alpha_0)\, \mathrm{d}\omega \tag{126}$$

In order to close Eq. (126), we must specify the relation between $K(\sigma)$ and $\mathrm{d}\bar{m}/\mathrm{d}\omega(\omega)$. If we assume that the relation between $K(\sigma)$ and $\mathrm{d}\bar{m}/\mathrm{d}\omega(\omega)$ is the same here as it is in the case of simple oscillators, then such a closure relation can be obtained from Eqs. (35) and (65). This yields, (for $\mathrm{d}\bar{m}/\mathrm{d}\omega(\omega)$ analytic in the upper half ω-plane)

$$K(\sigma) = -\frac{\pi}{2}\sigma^3 \frac{\mathrm{d}\bar{m}}{\mathrm{d}\omega}(\omega)\bigg|_{\omega=i\sigma}. \tag{127}$$

We combine Eqs. (126) and (127) to find the following homogeneous nonlinear integral equation for $\mathrm{d}\bar{m}/\mathrm{d}\omega(\omega)$:

$$\frac{\mathrm{d}\bar{m}}{\mathrm{d}\omega}(i\sigma) = \int_0^\infty \frac{\mathrm{d}\bar{m}}{\mathrm{d}\omega}(\omega) \frac{\mathrm{d}\bar{m}}{\mathrm{d}\omega}\left(\frac{i\sigma}{\omega}\right) \frac{\mathrm{d}\omega}{\omega}. \tag{128}$$

To solve Eq. (128), we replace $z = \log(i\sigma)$, $v = \log\omega$ and $\mu(z) = \mathrm{d}\bar{m}/\mathrm{d}\omega(\mathrm{e}^z)$ to write:

$$\mu(z) = \int_{-\infty}^\infty \mu(v)\mu(v - z)\, \mathrm{d}v. \tag{129}$$

Eq. (129) may be solved by Fourier transform. We denote by $\bar{\mu}$ the transform of μ. Taking the transform of Eq. (129) leads to

$$\bar{\mu} = \bar{\mu}^2 \tag{130}$$

$$\bar{\mu} = 1 \tag{131}$$

Thus, we conclude that

$$\frac{\mathrm{d}\bar{m}}{\mathrm{d}\omega}(\omega) = \delta(\omega - \omega_0). \tag{132}$$

Eq. (132) describes the mass-frequency distribution of a single oscillator with arbitrary natural frequency ω_0. The implication of Eq. (132) is that only *identical oscillators* can be connected together (in the manner that we have assumed) such that the behavior of whole is the same as the behavior of the individual parts.

Clearly the mass-frequency distribution in Eq. (132) is not representative of whole classes of complicated subsystems. While this result is not of practical interest, it is of interest to see where the assumption of self-similarity has led. We note, however, that self-similarity was not the only assumption made in this section, and that perhaps the concept of self-similarity might still lead to valuable subsystem models.

6.4. Rational function approximation

Here we consider representing $\mu(v)$ by a rational function of v. This representation has considerable benefits in terms of both ease of application and in terms of physical interpretation.

To obtain a rational function representation of $\mu(v)$, we must first choose a desirable form. We shall choose $\mu(v)$ to be an even function of v. In order that the integral in Eq. (105) be well defined, we require that $\mu(v)$ be $o(v^{-3})$ $v \to \infty$. These requirements lead us to choose the following form for $\mu(v)$:

$$\mu(v) = \frac{c}{(v^4 - 2(a^2 - b^2)v^2 + (a^2 + b^2)^2)}. \tag{133}$$

We note that more elaborate choices of $\mu(v)$ can lead to higher order models with (presumably) greater accuracy than that chosen here, however, Eq. (133) shall suffice to satisfy our three conditions (103)–(105).

6.4.1. Evaluating the coefficients a, b and c

The three coefficients in Eq. (133) are to be determined by requiring Eq. (133) to satisfy Eqs. (103)–(105). This leads to the equations (Mathematica was used here)

$$1 = \frac{\pi c}{4b(a^2 + b^2)} \tag{134}$$

$$\alpha_0 = \frac{c}{4ab}[\pi - 2\theta] \tag{135}$$

$$1 = \frac{\pi c}{4b}. \tag{136}$$

In Eq. (135), θ is defined so that $\tan\ \theta = b/a$. Solving Eqs. (134) and (136) in terms of θ yields

$$a = \cos\ \theta \tag{137}$$

$$b = \sin\ \theta \tag{138}$$

$$c = 4/\pi\ \sin\ \theta \tag{139}$$

The value of θ is determined from Eq. (135) which simplifies using Eqs. (137)–(139) to

$$\frac{\pi - 2\theta}{\pi\ \cos\ \theta} = \alpha_0. \tag{140}$$

Thus, given α_0 for a particular subsystem, we determine θ by solving Eq. (140). Then we obtain a, b and c from Eqs. (137)–(139). We note that Eq. (140) has real solutions for θ only for $\alpha_0 > 2/\pi$. Smaller values of α_0 can be obtained by allowing $\theta = \pi/2 + i\gamma$, as we shall discuss later.

6.4.2. Implementation of rational function approximation

The rational function approximation can be implemented in either convolution form, or in a form local in time. To obtain the convolution form, we merely substitute $\mu(v)$ into Eq. (24). Since the kernel is a rational function of v, however, the resulting DtN map can be written alternatively in a form that is local in time.

To show this, we consider the non-dimensional DtN map in the Laplace domain. Therefore we introduce $\bar{K}(\sigma)$ which is the non-dimensional Laplace transform of the approximate DtN map resulting from $\bar{m}(\omega)$ (cf Eqs. (31), (32) and (67)).

$$\bar{K}(\sigma) = 1 - \int_0^\infty \int_0^\infty v^3 \mu(v)\ \sin(v\tau)\ \mathrm{d}v\ \mathrm{e}^{-\sigma\tau}\ \mathrm{d}\tau = 1 - \int_0^\infty \mu(v) \frac{v^4}{\sigma^2 + v^2}\ \mathrm{d}v \tag{141}$$

Here, $\bar{K}$ is non-dimensionalized with respect to k_o, and σ is non-dimensionalized with respect to Ω. Thus with the definition (141), Eq. (31) becomes:

$$F_0(s) = s^2 m_o X_0(s) + k_o \bar{K}(s/\Omega) X_0(s). \tag{142}$$

When $\mu(v)$ is a rational even function, as here, the integral (141) is easily evaluated by residues. The result is a rational function of σ of the form (Mathematica used here):

$$\bar{K}(\sigma) = 1 - N(\sigma)/D(\sigma) \tag{143}$$

$$N(\sigma) = (1 + 2b\sigma) \tag{144}$$

$$D(\sigma) = (\sigma^2 + 2b\sigma + 1). \tag{145}$$

We now substitute Eq. (143) into Eq. (142), multiply both sides by $D(\sigma)$, and inverse Laplace transform to obtain:

$$\mathscr{D} f_0(t) = m_o \frac{\mathrm{d}^2}{\mathrm{d}t^2} \mathscr{D} x_0(t) + k_o \frac{\mathrm{d}^2}{\mathrm{d}t^2} x_0(t). \tag{146}$$

The operator $\mathscr{D}$ is given by:

$$\mathscr{D} = \frac{\mathrm{d}^2}{\mathrm{d}t^2} + 2b\Omega \frac{\mathrm{d}}{\mathrm{d}t} + \Omega^2. \tag{147}$$

The form of the DtN map, Eq. (146), is much more convenient in implementation than the convolution form. For one, it does not require the full displacement history at the attachment point. Further, the evaluation of the force $f_0(t)$ at each time step is relatively efficient compared to a long time convolution. We shall show below an equivalent formulation which is not only local in time, but has an appealing physical analogy.

Before closing this section, we note that the form (146) with the coefficients as given is subject to the restriction of homogeneous initial conditions on $f(t)$ and $x_0(t)$:

$$f_0(0) = 0 \quad \dot{f}_0(0) = 0$$

$$x_0(0) = 0 \tag{148}$$

6.4.3. A physical analogy

In this section, we describe a simple model which corresponds to the local (in time) DtN map, Eq. (146). To start with, we rewrite Eq. (146) as

$$f_0(t) = m_o \frac{\mathrm{d}^2}{\mathrm{d}t^2} x_0(t) + f_2(t), \tag{149}$$

$$\mathscr{D} f_2(t) = k_o \frac{\mathrm{d}^2}{\mathrm{d}t^2} x_0(t). \tag{150}$$

We now introduce a 'dummy' displacement-type variable, $y(t)$, defined by

$$f_2(t) = M_T \ddot{y}(t); \quad y(0) = \dot{y}(0) = 0. \tag{151}$$

Substituting Eq. (151) into Eq. (150) and integrating twice with zero initial conditions yields:

$$M_T \ddot{y}(t) + 2bM_T \Omega \dot{y}(t) + k_o y(t) = k_o x(t). \tag{152}$$

Eq. (152) is the equation of motion for a spring-dashpot-mass system in series. The parameters M_T and k_o are the mass and spring constants of mass-spring system, respectively. The coefficient b defined in Eq. (138) has the physical interpretation of the fraction of critical damping. This implies that the dashpot constant C in the analogy is given by

$$C = M_T \Omega / 2b = k_o / 2b\Omega \tag{153}$$

We emphasize that the physical analogy is exactly equivalent to the local DtN map resulting from the rational function representation of $\bar{m}(\omega)$.

In terms of the 'dummy' displacement variable $y(t)$, the local DtN map, Eqs. (149) and (150) can now be rewritten as:

$$f_0(t) = m_o \frac{\mathrm{d}^2}{\mathrm{d}t^2} x_0(t) + M_T \ddot{y}(t), \tag{154}$$

$$k_o x(t) = M_T \ddot{y}(t) + 2bM_T \Omega \dot{y}(t) + k_o y(t). \tag{155}$$

Eqs. (154) and (155) are in the most convenient form for practical implementation.

6.4.4. Relation between critical damping parameter and effective dissipation parameter

It is interesting to examine the relation between the critical damping parameter b from the physical analogy and the effective dissipation parameter α_0 that results from the high modal density approximation. These two can be related through Eqs. (138) and (140).

Underdamped case: Provided $b \leq 1$, α_0 and b are related by:

$$\alpha_0 = \frac{\pi - 2 \sin^{-1} b}{\pi \sqrt{1 - b^2}}. \tag{156}$$

Overdamped case: When $b \geq 1$, Eq. (156) is still valid, but can be rewritten in a much more convenient form. We shall use the identity

$$\sin^{-1}x = \pi/2 + i\,\cosh^{-1}x. \tag{157}$$

Thus, Eq. (156) simplifies to

$$\alpha_0 = \frac{2\,\cosh^{-1}b}{\pi\sqrt{b^2-1}}. \tag{158}$$

The two relations (156) and (158) are summarized in the plot in Fig. 2.

6.4.5. Estimated bounds on critical damping parameter

In Section 4.2 we showed that $K(s)$ is bounded by its Padé approximants. We have no such bounds on $\bar{K}(\sigma)$, however. It is interesting, nevertheless, to assume that those bounds derived in Section 4.2 hold for $\bar{K}(\sigma)$, and thus derive estimated bounds for the critical damping factor, b. Therefore, based on Eq. (38) we shall assume:

$$P_1^0(s^2) \le k_o\bar{K}(s/\Omega) \le P_1^1(s^2). \tag{159}$$

We use the high frequency derivation of P_1^0 given by Eq. (57) and the low frequency expression for P_1^1 given by Eq. (46) in Eq. (159) to write

$$\frac{k_o^2}{k_o + s^{-2}\sum_{n=1}^{N} m_n\omega_n^4} \le k_o\bar{K}(s/\Omega) \le \frac{s^2M_T^2}{M_T + s^2\sum_{n=1}^{N}(m_n/\omega_n^2)}. \tag{160}$$

We gain some confidence in our assumption of Eq. (159) by the fact that Eq. (160) is satisfied in both the $s = 0$ and $s=\infty$ limits.

To obtain bounds on b, we substitute Eqs. (143)–(145) into Eq. (160) and evaluate the result at $s=\Omega$ to obtain:

$$\frac{k_o^2}{k_o + \Omega^{-2}\sum_{n=1}^{N} m_n\omega_n^4} \le \frac{k_o}{2+2b} \le \frac{M_T^2\Omega^2}{M_T + \Omega^2\sum_{n=1}^{N}(m_n/\omega_n^2)}. \tag{161}$$

Simplifying leads to

$$\frac{\sum_{n=1}^{N}(m_n/\omega_n^2)}{M_T/\Omega^2} - 1 \le 2b \le \frac{\sum_{n=1}^{N} m_n\omega_n^4}{M_T\Omega^4} - 1. \tag{162}$$

The inequality (47), however, shows the left hand side of Eq. (162) to be non-positive. The inequality in Eq. (63), on the other hand, shows the right hand side of Eq. (162) to be always non-negative. Thus we obtain the estimated bound on the critical damping coefficient, b:

$$0 \le 2b \le \frac{\sum_{n=1}^{N} m_n\omega_n^4}{M_T\Omega^4} - 1. \tag{163}$$

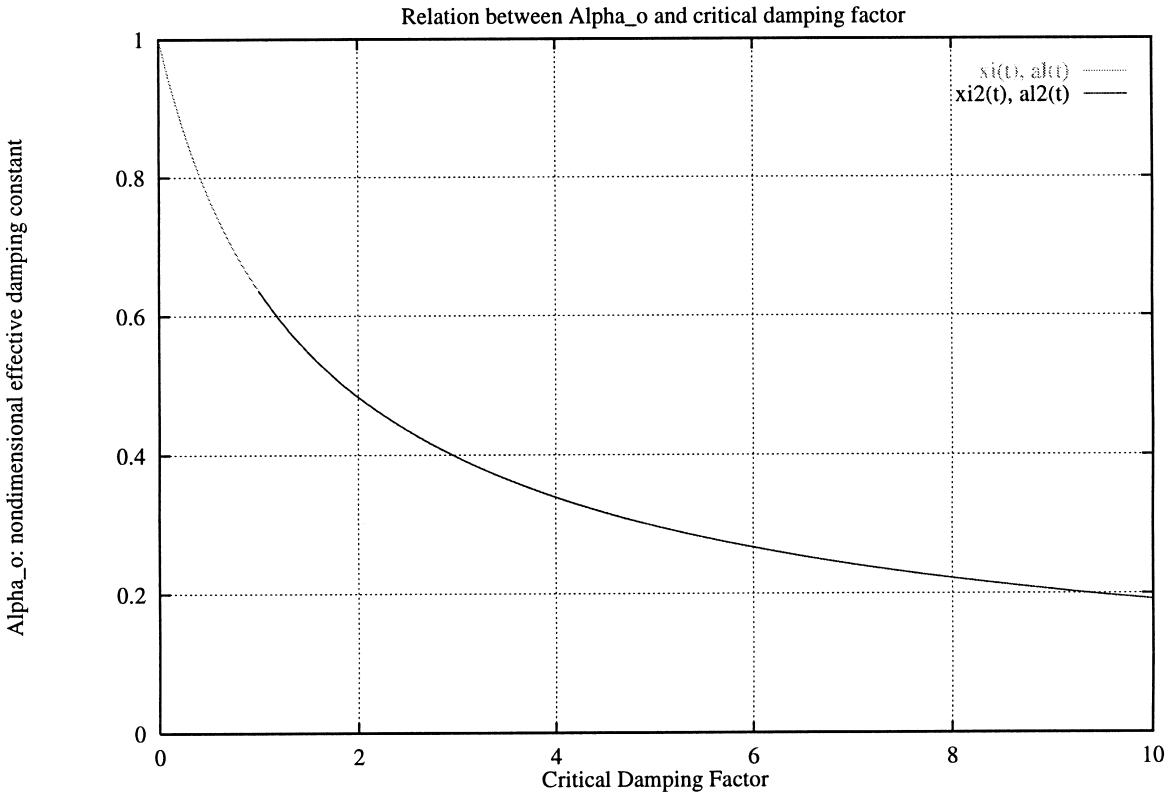

Fig. 2. Relation between critical damping factor, b, and 'effective' damping constant, α_0. The relation is described quantitatively in Eqs. (156) and (158).

7. Examples

In the examples that follow, we shall remove a large portion of the computational problem and replace it with a DtN boundary condition as we have described earlier. The DtN map shall be computed with a high-modal density approximation. The results of using the DtN map shall be compared to results obtained by simulating the full dynamical system.

7.1. Large oscillator connected to complicated substructure

The first system that we shall consider is that studied by Weaver (1996, 1997). It consists of a 'large' mass-spring oscillator which is attached to a complicated substructure, as shown in Fig. 3. The equations of motion for the system are

$$M\ddot{x}_0(t) + Kx_0(t) = \sum_{n=1}^{N} \kappa_n (x_n(t) - x_0) \tag{164}$$

$$m_n \ddot{x}_n(t) + \kappa_n x_n(t) = \kappa_n x_0(t) \tag{165}$$

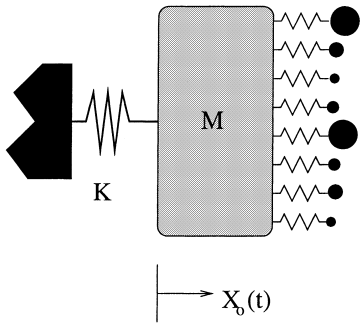

Fig. 3. A large mass-spring oscillator connected to a complicated substructure. The substructure is represented by the collection of small oscillators.

$$k_o = \sum_{n=1}^{N} \kappa_n. \tag{166}$$

7.1.1. Exact DtN map formulation

In order to apply the DtN map concept, we rewrite Eqs. (164)–(166) as follows:

$$M\ddot{x}_0(t) + Kx_0(t) = -f_0(t) \tag{167}$$

$$f_0(t) = \sum_{n=1}^{N} \kappa_n (x_n(t) - x_0) \tag{168}$$

To make the connection to our original formulation, we note that Eq. (165) is identical to Eq. (7), Eq. (166) is a special case of Eq. (5), and Eq. (168) is a special case of Eq. (8).

In this example, $m_o = 0$, $\omega_n^2 = \kappa_n/m_n$, $M_T = \Sigma_n m_n$, $\Omega^2 = k_o/M_T$. Thus, Eq. (24) gives us the force as:

$$f_0(t) = k_o x_0(t) - \int_{-\infty}^{t} \sum_{n=1}^{N} m_n \omega_n^3 \ \sin\ \omega_n(t-\tau) x_0(\tau)\, d\tau. \tag{169}$$

Therefore, in order to determine the dynamic response of the mass, we must solve Eq. (167) with Eq. (169), subject to initial conditions

$$x_0(0) = A; \quad \dot{x}_0(0) = B. \tag{170}$$

7.1.2. Approximate DtN map formulation

Alternatively, we can use the approximate DtN map, Eqs. (154) and (155). For this example, Eqs. (154) and (155) simplify to

$$f_0(t) = k_o x_0(t) - 2bM_T\Omega\dot{y}(t) - k_o y(t), \tag{171}$$

$$k_o x_0(t) = M_T\ddot{y}(t) + 2bM_T\Omega\dot{y}(t) + k_o y(t). \tag{172}$$

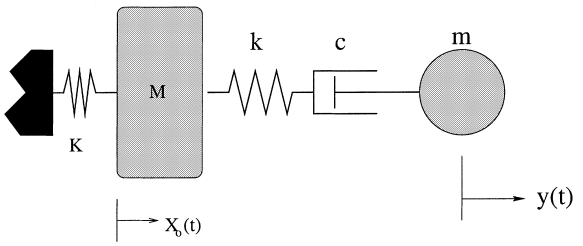

Fig. 4. The asymptotically equivalent system. The response of the master structure in this system is approximately the same as that depicted in Fig. 3. The substructure has been replaced by a spring-dashpot-mass structure.

Combining Eq. (171) with Eq. (167) yields

$$M\ddot{x}_0(t) + (K + k_o)x_0(t) = 2bM_T\Omega\dot{y}(t) + k_o y(t). \tag{173}$$

Therefore, in order to determine the approximate dynamic response of the mass, we must solve Eq. (173) with Eq. (172), subject to initial conditions (170) and

$$y(0) = 0; \quad \dot{y}(0) = 0. \tag{174}$$

The differential Eqs. (173) with (172) exactly represent the system depicted in Fig. 4.

To evaluate the constant b, we must first evaluate η_o which is given by Eq. (96) as

$$\eta_o = \sum_{n=1}^{N} \omega_n m_n. \tag{175}$$

Then, $\alpha_0 = \eta_o / M_T\Omega$ (by Eq. (100)) and b can be evaluated by solving either Eq. (156) or Eq. (158), as appropriate.

7.1.3. Example results

Here we compare the results for a subsystem of $N = 1000$ masses attached to a single large mass. We compare the results of the approximate DtN map, Eq. (173) with Eq. (172), to the results obtained by directly simulating the full system of Eqs. (164)–(166).

The large mass is $M = 2$, while its spring has spring constant $K = 2$. The values of ω_n were chosen randomly between 0 and $\Omega_{\max} = 10$. The values of m_n were chosen according to a selected distribution, as

$$m_n = p(\omega)\Omega_{\max}/N. \tag{176}$$

In all the examples, $p(\omega)$ is chosen to be $p(\omega) = M_T \exp(-\lambda\omega)/\lambda$, with $\lambda = 2.0$. For the dynamical simulations, the initial conditions are given by Eqs. (170) and (174), with $A = 0$ and $B = 1$.

We consider two different subsystems with very different masses. In one case, the subsystem has mass $M_T \approx 0.25$, while in the other case $M_T \approx 10$. The two results are shown in Figs. 5 and 6, respectively. We note that remarkably different physical behavior results in the two cases. In each case, however, we see that the approximate solution, obtained from integrating just two second order equations, closely approximates the reference solution for times below about 50 units. Above those times, the approximation breaks down as predicted by the error analysis in Section 5.3.1.

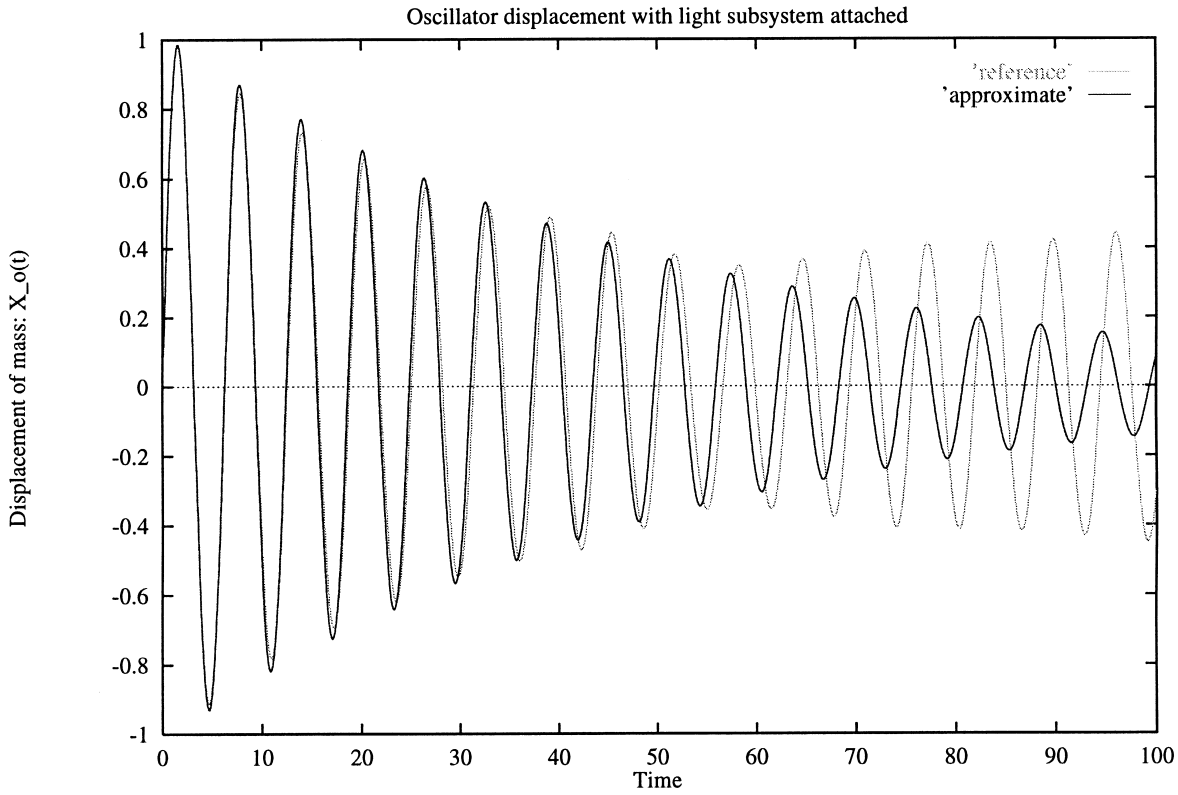

Fig. 5. Example 1a: 'large' mass-spring oscillator interacting with light but complicated substructure.

7.2. Elastic rod connected to complicated substructure

We now consider the interaction between two elastic structures: a homogeneous elastic rod connected to a 'complicated', randomly inhomogeneous elastic rod; see Fig. 7. We shall represent the inhomogeneous rod using a high-modal density DtN map as we did in the last example. Indeed, to model the inhomogeneous rod, we follow steps similar to those outlined above.

In Fig. 8, we plot the displacement profiles on the homogeneous portion of the rod at even time intervals. We plot the displacement predicted by the approximate DtN map and compare that to the displacement predicted in the reference structure. The input is a Gaussian shaped pulse which propagates to the right. The right traveling wave is represented at 25 time-unit intervals by the large peaks centered at $x = 10$, 35, 60 and 85. (The wave speed in the homogeneous rod is unity.) The right traveling pulse is reflected at the right end of the homogeneous rod. The reflected left traveling pulse is of lower amplitude.

We see that the approximate and reference solutions agree exactly up to the reflection from the complicated substructure. The subsequent reflected pulses agree closely in shape and amplitude. The main difference between them is represented in the slow decay of the tail in the approximate solution. The elapsed time shown in the figures is not sufficient to show the pulse reflected from the far end of the complicated rod. The approximate solution does *not* predict this pulse, though it is present in the reference solution, of course.

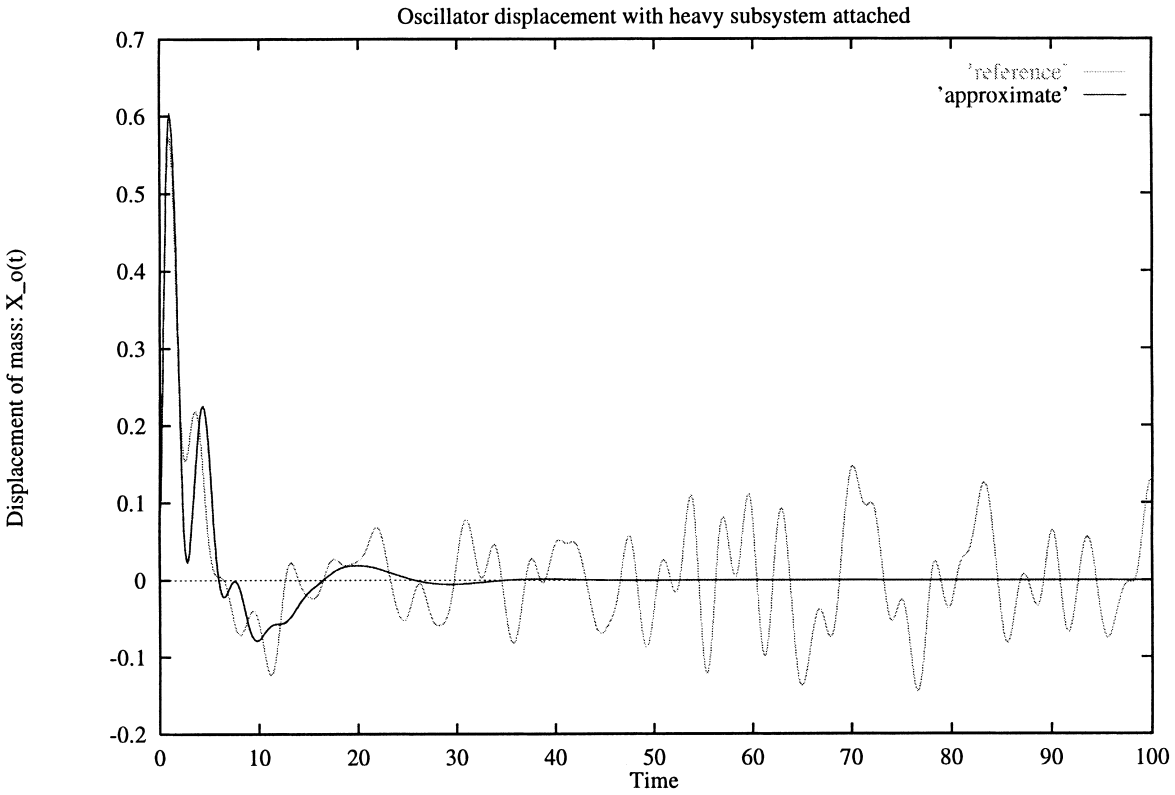

Fig. 6. Example 1b: 'large' mass-spring oscillator interacting with heavier complicated substructure.

8. Conclusions

We have proposed the use of a time-domain DtN map to represent complicated subsystems in dynamical simulations. We derived an exact DtN map for a general linear-elastic system which is attached to the outside world at one point. We studied the properties of this map and found many interesting results including interrelations between bulk dynamical coefficients, and bounds on the

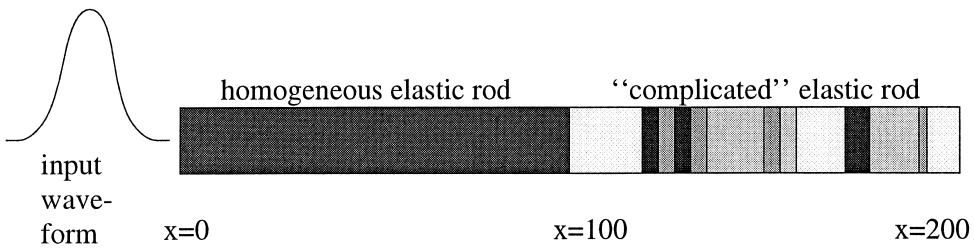

Fig. 7. A homogeneous elastic rod connected to an inhomogeneous elastic rod. The homogeneous rod is the main structure of interest. The effect of the 'complicated' inhomogeneous rod on the dynamics of the other shall be represented by an approximate DtN map.

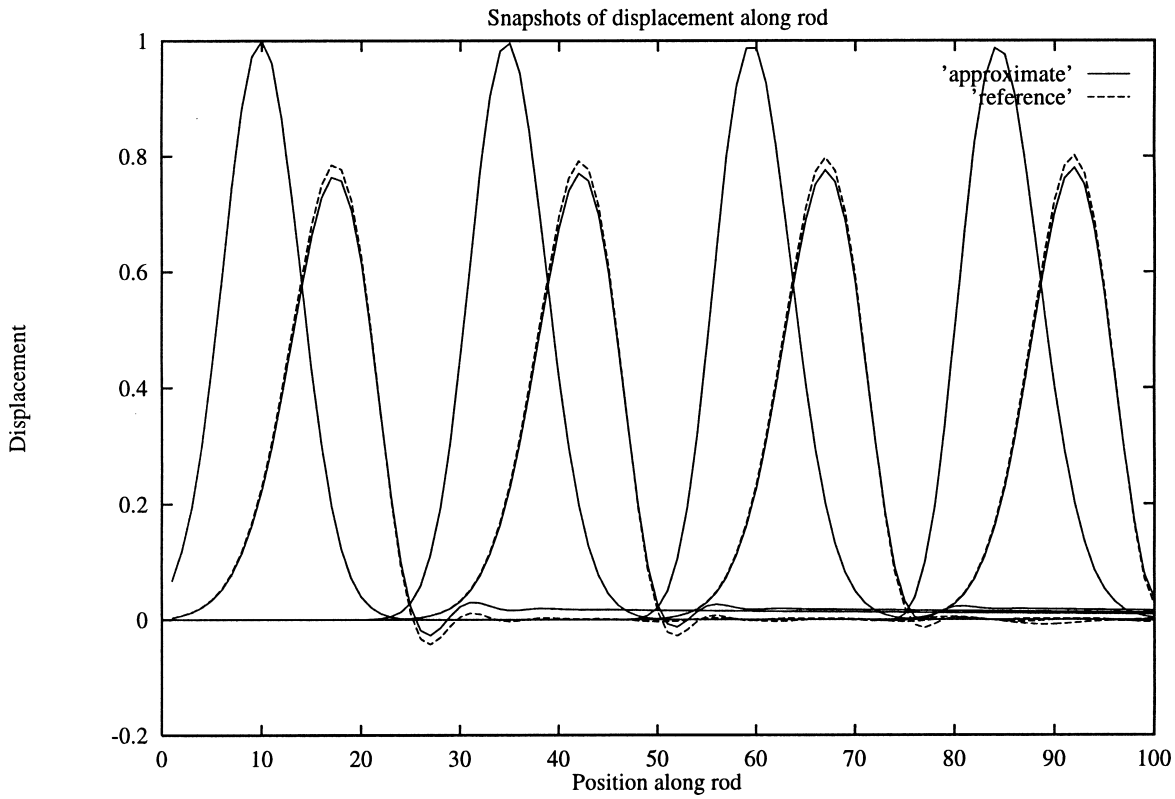

Fig. 8. Example 2: reflection from elastic bar with random mass density.

symbol of the map in the Laplace domain. We also studied the high modal density or infinitely complicated limit, and derived the 'effective dynamical parameters' governing the dynamics of a subsystem. These were used to construct various subsystem representations which are accurate in the high modal density limit. The most intriguing of these is the rational function representation. From this representation we were lead to conclude that a sufficiently complicated subsystem is asymptotically equivalent (as $\epsilon \to 0$) to a simple single spring-dashpot-mass system, (for $t = o(\epsilon^{-1})$.) Several examples of our high modal density approximation were studied. The agreement between model and reference solutions was initially very good, but gradually deteriorated in agreement with the predictions of Section 5.3.1.

The results presented here show that a sufficiently complicated subsystem can be accurately represented by a subsystem of much smaller dimensionality. The model system is dissipative, even though the original system is not. The dissipation models vibratory energy being transferred from the master structure to the slave subsystem (Pierce et al., 1993; Strasberg and Feit, 1996). This analogy provides an interesting dynamical interpretation of the origin of damping in physical systems.

Though our analysis is presented in the context of structural dynamics, it generally applies to any large system of oscillators. We emphasize, however, that the high modal density approximation presented here is valid only for simulation time $= o(\epsilon^{-1})$. Cherukuri and Barbone (1998) show that small dissipation of $O(\epsilon)$ in the subsystem is sufficient to keep the high modal density approximation valid for all time. Essentially, the dissipation kills the response before the error has time to build up. Developing

an approximation which is valid for all time in the absence of dissipation is more difficult, and is an area of active work.

Acknowledgements

The authors acknowledge helpful discussions with Ofer Michael, Karl Grosh, Jeffrey L. Cipolla, Donald Cox, Charles Milligan, Geoffrey Main, and Allan D. Pierce. The finanical support of the Office of Naval Research is also gratefully acknowledged.

Appendix A. Proof that $\alpha_0 \leq 1$ for all subsystems

In this Appendix, we prove that $\alpha_0 \leq 1$ for all subsystems. The proof proceeds by induction. We first show that for a system with a single mode, $\alpha_0 = 1$. The we show if $\alpha_0 \leq 1$ for a system with N modes of vibration, then $\alpha_0 \leq 1$ with the addition of another mode of vibration.

We recall the definition α_0 given in Eq. (100)

$$\alpha_0 = \eta_o / M_T \Omega > 0. \tag{A1}$$

Here, $\Omega^2 = k_o/M_T$, and M_T, η_o, k_o are the 'effective dynamical parameters' defined in Eqs. (96)–(98).

Here we consider the values of M_T, η_o, k_o as functions of N. To that end, we define:

$$M_N = \sum_{n=1}^{N} m_n \tag{A2}$$

$$\eta_N = \sum_{n=1}^{N} m_n \omega_n \tag{A3}$$

$$k_N = \sum_{n=1}^{N} m_n \omega_n^2 \tag{A4}$$

$$\Omega_N^2 = k_N / M_N \tag{A5}$$

$$\alpha_N = \eta_N / M_N \Omega_N \tag{A6}$$

To begin, we let $N = 1$ in Eqs. (A2)–(A6) to find

$$\alpha_1 = 1. \tag{A7}$$

From Eqs. (A2)–(A4), we now note

$$M_{N+1} = M_N + m_{N+1} \tag{A8}$$

$$\eta_{N+1} = \eta_N + m_{N+1} \omega_{N+1} \tag{A9}$$

$$k_{N+1} = k_N + m_{N+1}\omega_{N+1}^2. \tag{A10}$$

Thus we can write the following equation for α_{N+1}^2:

$$\alpha_{N+1}^2 = \frac{\eta_{N+1}^2}{M_{N+1}k_{N+1}} \tag{A11}$$

$$= \frac{\alpha_N^2 + 2\alpha_N \dfrac{m_{N+1}}{M_N}\dfrac{\omega_{N+1}}{\Omega_N} + \dfrac{m_{N+1}^2}{M_N^2}\dfrac{\omega_{N+1}^2}{\Omega_N^2}}{\left(1+\dfrac{m_{N+1}}{M_N}\right)\left(1+\dfrac{m_{N+1}}{M_N}\dfrac{\omega_{N+1}^2}{\Omega_N^2}\right)}. \tag{A12}$$

For convenience, we are motivated to introduce the following variables:

$$\mu = m_{N+1}/M_N \quad v = \omega_{N+1}/\Omega_N. \tag{A13}$$

We note that these definitions hold in this appendix only, and are not to be confused with the definitions of μ and v given in the main text of the paper.

In terms of μ and v, Eq. (A12) can be rewritten as

$$\alpha_{N+1}^2 = \frac{\alpha_N^2 + 2\alpha_N\mu v + \mu^2 v^2}{(1+\mu)(1+\mu v^2)}. \tag{A14}$$

From Eq. (A14), we conclude:

$$\alpha_{N+1}^2 > 1 \;\Leftrightarrow\; \alpha_N^2 + 2\alpha_N\mu v + \mu^2 v^2 > (1+\mu)(1+\mu v^2). \tag{A15}$$

Simplifying the right hand side of Eq. (A15) yields:

$$\alpha_{N+1}^2 > 1 \;\Leftrightarrow\; \alpha_N^2 + 2\mu v\alpha_N - (1+\mu(1+v^2)) > 0. \tag{A16}$$

We shall now show that $\alpha_N^2 + 2\mu v\alpha_N - (1+\mu(1+v^2)) > 0$ is not satisfied for any $0 < \alpha_N \leq 1$.

We let α^* be the positive root of

$$\alpha^{*2} + 2\mu v\alpha^* - (1+\mu(1+v^2)) = 0. \tag{A17}$$

It is easy to show that the second root of Eq. (A17) is negative. α^* is given by:

$$\alpha^* = \sqrt{(1+\mu v)^2 + \mu(1-v)^2} - \mu v \geq \sqrt{(1+\mu v)^2} - \mu v = 1. \tag{A18}$$

Finally, we note that $\alpha_N = 0$ leads to the right hand side of Eq. (A16) being false.

We conclude that

$$\alpha_{N+1}^2 > 1 \Leftrightarrow \alpha_N > \alpha^* \geq 1. \tag{A19}$$

Thus, $\alpha_{N+1} > 1$ if, and only if, $\alpha_N > 1$. Since $\alpha_1 = 1$, α_2 and all subsequent α_n's will be equal to or less than unity.

It is worth noting before we close this section that the equality in Eq. (A18) is achieved only for $v = 1$.

References

Abramowitz, M., Stegun, I.A., 1972. Handbook of Mathematical Functions, Dover Publications, New York.

Barbone, P.E., 1995. Equipment representations for shock calculations: time domain Dirichlet to Neumann maps. In: Proceedings of 1995 Design Engineering Technical Conferences, Acoustics, Vibrations, and Rotating Machines, Boston, MA, September 1995, 3, Part B. ASME Press, New York, pp. 223–228.

Barbone, P.E., 1998. Effective dynamical properties. In: Proceedings of ASME Noise Control and Acoustic Division, 1998 International Mechanical Engineering Congress, Anaheim, CA, November 1998, NCA25. ASME Press, New York, pp. 333–338.

Bender, C.M., Orszag, S.A., 1978. Advanced Mathematical Methods of Scientists and Engineers, (International edition) ed. McGraw-Hill, Singapore.

Cherukuri, A., Barbone, P.E., 1998. High modal density approximations for equipment in the time domain. J. Acoust. Soc. Am. 104 (4), 2048–2053.

Craig, R.R., 1995. Substructure methods in vibration. Trans. ASME J. Vib. Acoust. 117 (3), 207–213.

Givoli, D., 1990. A combined analytic-finite element method for elastic shells. Int. J. of Solids and Structures 26, 185–198.

Givoli, D., 1992. Numerical Methods for Problems on Infinite Domains, 1st ed. Elsevier, Amsterdam.

Givoli, D., Keller, J.B., 1989. A finite element method for large domains. Comput. Meth. Appl. Mech. Engng 76, 41–66.

Givoli, D., Keller, J.B., 1990. Non-reflecting boundary conditions for elastic waves. Wave Motion 12, 261–279.

Givoli, D., Keller, J.B., 1992. A finite element method for domains with corners. Int. J. for Numerical Methods in Engineering 35, 1329–1345.

Givoli, D., Rivkin, L., 1993. The DtN finite element method for elastic domains with cracks and reentrant corners. Computers and Structures 49, 633–642.

Goldman, D., Barbone, P.E., 1996. Dirichlet to Neumann maps for the representation of equipment with weak non-linearities. In: Proceedings of ASME Noise Control and Acoustics Division, 1996 International Mechanical Engineering Congress, Atlanta, GA, November 1996, NCA22. ASME Press, New York, pp. 71–76.

Guyan, R.J., 1965. Reduction of stiffness and mass matrices. AIAA Journal 3 (2), 380.

Hurty, W.C., 1965. Dynamic analysis of structural systems using component modes. AIAA Journal 3 (4), 678–685.

Keller, J.B., Givoli, D., 1989. Exact non-reflecting boundary conditions. J. Comput. Phys. 82, 172–192.

Lanczos, C., 1986. The Variational Principles of Mechanics. Dover (Reprint of fourth (1970) edition).

Nagem, R.J., Veljkovic, I., Sandri, GvH, 1997. Vibration damping by a continuous distribution of undamped oscillators. J. Sound Vib. 207 (3), 429–434.

O'Hara, G.J., Cunniff, P.F., 1963. Elements of normal mode theory. Naval Research Laboratory Report No. 6002.

Pierce, A.D., Sparrow, V.W., Russel, D.A., 1993. Fundamental structural-acoustic idealizations for structures with fuzzy internals. In: Proceedings of ASME Winter Annual Meeting, New Orleans, November 1993, ASME Transactions, Paper No. 93-WA/NCA-17.

Pierce, A.D., 1995a. Resonant-frequency-distribution of internal mass inferred from mechanical impedance matrices, with application to fuzzy structure theory. In: Proceedings of the ASME Symposium on Acoustics of Submerged Structures and Transduction Systems, 17–21 September 1995. ASME Press, New York.

Pierce, A.D., 1995b. Fuzzy elements, their coupling rules, and the Jaynes-Shannon maximum entropy principle. Technical Report AM-95-032, Department of Aerospace and Mechanical Engineering, Boston University, November 1995.

Strasberg, M., Feit, D., 1996. Vibration damping of large structures induced by attached small resonant structures. J. Acoust. Soc. Am. 99 (1), 335–344.

Weaver, R.L., 1996. The effect of an undamped finite degree of freedom 'fuzzy' substructure: numerical solutions and theoretical discussion. J. Acoust. Soc. Am. 100 (5), 3159–3164.

Weaver, R.L., 1997. Mean and mean-square responses of a prototypical master/fuzzy structure. J. Acoust. Soc. Am. 101 (3), 1441–1449.